

EXPERIMENTATION OF ABRASION EROSION AT HIGH TEMPERATURE FOR  
CONCENTRATED SOLAR POWER SYSTEMS

by

Tessa Mei-lin Fong



A thesis

submitted in partial fulfillment

of the requirements for the degree of

Master of Science in Mechanical Engineering

Boise State University

May 2022

© 2022

Tessa Mei-lin Fong

ALL RIGHTS RESERVED

BOISE STATE UNIVERSITY GRADUATE COLLEGE

**DEFENSE COMMITTEE AND FINAL READING APPROVALS**

of the thesis submitted by

Tessa Mei-lin Fong

Thesis Title: Experimentation of Abrasion Erosion at High Temperature in Concentrated Solar Power Systems

Date of Final Oral Examination: 10 March 2022

The following individuals read and discussed the thesis submitted by student Tessa Mei-lin Fong, and they evaluated the student's presentation and response to questions during the final oral examination. They found that the student passed the final oral examination.

Todd P. Otanicar, Ph.D. Chair, Supervisory Committee

Mahmood Mamivand, Ph.D. Member, Supervisory Committee

Krishna Pakala, Ph.D. Member, Supervisory Committee

The final reading approval of the thesis was granted by Todd P. Otanicar, Ph.D., Chair of the Supervisory Committee. The thesis was approved by the Graduate College.

## DEDICATION

This thesis is dedicated to my favorite sister, Violet Fong. She has been a huge support throughout both my undergraduate and graduate work. I could not have asked for a better cheerleader than her. I also would like to dedicate this thesis to my parents, Sharadon Smith and Edison Fong. Thank you for all your support.

## ACKNOWLEDGMENTS

I would first like to give my biggest acknowledgement and thanks to my thesis advisor, Dr. Todd Otanicar. He has been a huge support through my ups and downs during my master's and has shown me patience and given me the motivation I needed to complete this piece of work.

I would also like to acknowledge the rest of my committee members for their support, including Dr. Mahmood Mamivand and Dr. Krishna Pakala. Not only have they supported me during my thesis but also through my undergraduate degree. So, thank you for all your help!

Finally, I would like to acknowledge everyone regarding my project- the Department of Energy who funded this project, the people I worked with at Boise State University, including but not limited to Dr. Nipun Goel, Eyad Amoudi, and Andrew Russell, along with support from students and faculty at The University of Tulsa.

## ABSTRACT

Concentrated solar power (CSP) is an alternative and sustainable way to produce energy. Studies have shown that running these plants at high temperatures above 700°C can increase the thermal efficiency in heat transfer. Molten salt is usually used as the heat transfer medium but cannot be used due to its low maximum temperature and high freezing point. Running these plants at high temperature brings up the concern of erosion and oxidation. Abrasion erosion occurs through the interaction of particles and material. The goal of this research is to understand material degradation due to abrasion erosion to understand the durability of using solid particles as the heat transfer medium. Previous research has been done but not at the high temperature and low velocity to simulate these conditions. An apparatus was built to test the interaction of particles and materials at 800°C, periodically measuring the mass of each specimen and running a total of around 700 hours. Analysis for the specimen included calculating abrasion wear, surface profilometry, and cross-sectional scanning electron microscope imaging. Analysis for the particles included reflectance and particle size analysis. It was found temperature had the greatest effect on abrasion wear. For a test with silica quartz Wedload 430 particles and stainless steel 326H specimen, abrasion wear at 800°C and 25°C was  $-2.9281 \text{ mg/cm}^2$  and  $-0.1956 \text{ mg/cm}^2$ , respectively. There was no erosion of particles based on their circularity before and after testing.

Keywords: concentrated solar power, high temperature, abrasion, erosion, solid particles, oxidation, wear

## TABLE OF CONTENTS

DEDICATION .....	iv
ACKNOWLEDGMENTS .....	v
ABSTRACT .....	vi
LIST OF TABLES .....	xi
LIST OF FIGURES .....	xiii
LIST OF ABBREVIATIONS .....	xvii
CHAPTER ONE: INTRODUCTION .....	1
1.1 Motivation.....	1
1.2 Concentrated Solar Power Systems.....	2
1.3 Research Goals.....	5
CHAPTER TWO: BACKGROUND AND LITERATURE REVIEW.....	6
2.1 Introduction.....	6
2.2 Factors due to Abrasion Erosion.....	6
Erosion due to Velocity .....	7
Erosion due to Particle Shape and Size .....	8
Erosion due to Particle and Material Hardness/Ductility .....	10
2.3 Oxidation and Erosion at High Temperatures.....	11
Oxidation and Wear Basics.....	12
Oxidation in Stainless Steel .....	14

2.4	Testing of Abrasion Erosion and its Application to CSP Plants .....	16
	Abrasion Wear and Oxidation Experiment .....	16
	CSP Particle Receiver Experiment .....	18
2.5	Summary .....	20
CHAPTER THREE: DESIGN AND EXPERIMENTATION .....		24
3.1	Introduction .....	24
3.2	Abrasion Apparatus.....	24
	Speed of Rotation.....	26
3.3	Information on Particles and Specimens.....	27
	Specimen Material Information.....	27
	Particle Information .....	28
3.4	Preparation.....	28
	Specimen Preparation.....	28
	Oxidation Only Specimen Preparation.....	29
	Particle Preparation.....	30
3.5	Testing Instructions.....	30
	Set Up of Experiment.....	30
	Running the Experiments .....	30
3.6	Analysis Instructions.....	31
	Measuring Abrasion Wear.....	31
	Surface Profilometry.....	32
	Cross-Sectional Scanning Electron Microscope Images.....	33
	Reflectance .....	35

Optical Microscope and Particle Analysis.....	35
CHAPTER FOUR: RESULTS AND ANALYSIS .....	36
4.1 Introduction.....	36
4.2 Untested Particle Analysis .....	36
4.3 Thermocouple Verification.....	39
4.4 Abrasion Wear Results .....	41
Wear due to Erosion of Material.....	44
4.5 Effect of Temperature on Wear.....	44
High Temperature Creating Oxidation.....	44
Abrasion Wear in HT vs LT .....	49
4.6 Effect of Rotation at HT .....	54
Comparison of Weight Change due to Rotation .....	54
Oxidation and Rotation.....	57
4.7 Abrasion Wear Question Regarding SS316L .....	62
Error of Testing.....	64
SS316L Material .....	65
Cumulative Cycles .....	66
Increase of Oxides.....	68
4.8 Surface Profilometry on SS316L .....	69
4.9 Cross-Sectional SEM Imaging.....	70
Chemical Composition .....	72
4.10 Reflectance.....	73
4.11 Particle Size Analysis .....	74

4.12	Summary .....	77
CHAPTER FIVE: CONCLUSION.....		78
5.1	Work Completed.....	78
5.2	Limitations.....	79
5.3	Future Work.....	80
REFERENCES .....		82
APPENDIX A.....		85
APPENDIX B.....		104

## LIST OF TABLES

Table 2.1	Summary of research papers, the experiments, and the application. ....	22
Table 3.1	Information about materials used in experiments. ....	27
Table 3.2	Information about particles used in experiments. ....	28
Table 3.3	Information on how material specimens were cut and their dimensions. .	29
Table 4.1	Information on particles using in testing. ....	36
Table 4.2	Combinations of the different experiments ran.....	42
Table 4.3	Final average abrasion wear for each experiment.....	43
Table 4.4	Final average abrasion wear based on material specimen. ....	44
Table 4.5	Comparison of Galiullin’s test to the current testing parameters.....	55
Table 4.6	Synergy values of different specimens. ....	62
Table 4.7	Analysis of Surface Profilometry for SS316L .....	70
Table 4.8	Analysis of HSP 40/70 particles.....	76
Table A.1	Specimen mass of test with HSP 40/70 particles and SS316L and IN740H specimens at HT. ....	87
Table A.2	Specimen mass of test with HSP 40/70 particles and SS316L and IN740H specimens at LT. ....	88
Table A.3	Specimen mass of test with MAX HD 35 particles and SS316L and IN740H specimens at HT. ....	89
Table A.4	Specimen mass of test with MAX HD 35 particles and SS316L and IN740H specimens at LT.....	90
Table A.5	Specimen mass of test with WED 430 particles and HAY230 specimens at HT. Part 1.....	92

Table A.6	Specimen mass of test with WED 430 particles and HAY230 specimens at HT. Part 2 .....	93
Table A.7	Specimen mass of test with WED 430 particles and HAY230 specimens at LT. Part 1.....	95
Table A.8	Specimen mass of test with WED4 430 particles and HAY230 specimens at LT. Part 2.....	96
Table A.9	Specimen mass of test with HSP 40/70 #2 particles and SS316L specimens at HT.....	97
Table A.10	Specimen mass of test with WED 430 particles and SS316L and SS316H specimens at HT. Part 1.....	98
Table A.11	Specimen mass of test with WED 430 particles and SS316L and SS316H specimens at HT. Part 2.....	100
Table A.12	Specimen mass of test with WED 430 particles and SS316L and SS316H specimens at LT. Part 1 .....	101
Table A.13	Specimen mass of test with WED 430 particles and SS316L and SS316H specimens at LT. Part 2.....	102

## LIST OF FIGURES

Figure 1.1	Central receiver CSP system converting sunlight into electricity.....	2
Figure 1.2	Sketch of a falling particle receiver CSP system. ....	4
Figure 2.1	Effect of the velocity of silicon particles on steel metal at an angle of 20° [9]. ....	8
Figure 2.2	Erosion rate based on particle size. Edited from [11]. ....	9
Figure 2.3	Comparing erosion rate of Li's angular particles and Lin's rounded particles. Edited from [11]. ....	9
Figure 2.4	Erosion ratio of particles compared to their hardness [12]. ....	10
Figure 2.5	Volume loss of stainless steel 304 through different particle [14]. ....	11
Figure 2.6	Sketch of oxidation layer building up on a surface before breaking off [15]. ....	13
Figure 2.7	Sketch of oxide breaking off and a new oxidation layer forming on the surface [15]. ....	13
Figure 2.8	Testing of SS316L exposed to different temperatures over a period of time with no spalling removal [17]. ....	15
Figure 2.9	Testing of SS316L exposed to 800°C over a period of time while removing spalling [17]. ....	16
Figure 2.10	Sketch of apparatus showing specimen moving through particles. Units are in mm [18]. ....	17
Figure 2.11	Sample specimen and location of surfaces undergoing oxidation only ( <i>AOO</i> ) and abrasion and oxidation ( <i>AAO</i> ) [18]. ....	18
Figure 2.12	Set up of experiment to determine abrasion wear [19]. ....	19
Figure 2.13	Relative weight change vs exposure of martensitic steel VM12 [19]. ....	20
Figure 3.1	Schematic of apparatus being used for abrasion experiment. ....	25

Figure 3.2	Image of high temperature abrasion set up. ....	25
Figure 3.3	External Image of abrasion wear set up. ....	26
Figure 3.4	Sample specimen of where surface profilometry was taken. ....	32
Figure 3.5	Example of surface profilometry image (a) before and (b) after restoring data. ....	33
Figure 3.6	Sketch on where the specimen was cut for cross sectional SEM, shown by the red dotted line. ....	34
Figure 3.7	Image of specimen cut along the parallel and transverse lines to get a sample to epoxy. ....	34
Figure 4.1	Image of untested HSP 40/70 particles. ....	37
Figure 4.2	SEM image of untested HSP 40/70 particles. ....	37
Figure 4.3	Image of untested MAX HD 35 particles. ....	38
Figure 4.4	SEM image of untested MAX HD 35 particles. ....	38
Figure 4.5	Image of untested WED 430 particles. ....	39
Figure 4.6	SEM image of untested WED 430 particles. ....	39
Figure 4.7	Graph of thermocouple temperature compared to time. ....	40
Figure 4.8	Zoomed in image of thermocouple results found in Figure 4.7. ....	41
Figure 4.9	Abrasion wear graph of SS316L undergoing only oxidation. ....	46
Figure 4.10	Abrasion wear graph of IN740H undergoing oxidation only. ....	47
Figure 4.11	Abrasion wear graphs for HAY230 undergoing oxidation only. ....	48
Figure 4.12	Abrasion wear graphs for SS316H undergoing oxidation only. ....	49
Figure 4.13	Abrasion wear graphs of SS316H specimen effects on temperature. ....	50
Figure 4.14	Abrasion wear graph of IN740H specimens through HSP 40/70 particles. ....	51
Figure 4.15	Abrasion wear graph of IN740H specimens though MAX HD 35 particles. ....	52

Figure 4.16	Abrasion wear graph of SS316L specimens through MAX HD 35 particles.....	53
Figure 4.17	Abrasion wear graph of SS316L specimens through WED 430 particles.....	54
Figure 4.18	Averaged weight change of SS316L specimens through different particles compared to an edited graph of Galiullin’s work of martensitic steel from Figure 2.13.....	56
Figure 4.19	Abrasion wear of HAY230 specimen in WED 430 particles.....	58
Figure 4.20	Abrasion wear of SS316L specimen in WED 430 particles.....	59
Figure 4.21	Abrasion wear of SS316L specimen in HSP 40/70 #2 particles.....	60
Figure 4.22	Abrasion wear graph of SS316L running through MAX HD 35 particles.....	61
Figure 4.23	Abrasion wear of SS316L specimen for HT only.....	63
Figure 4.24	Abrasion wear graph of Figure 4.23 zoomed in.....	64
Figure 4.25	SS316L specimen in HSP 40/70 for HT to show effect of error.....	65
Figure 4.26	SS316L (a) rough and (b) smooth surface finishes.....	66
Figure 4.27	Abrasion wear vs cumulative cycles for SS316L specimen tests.....	67
Figure 4.28	Image of HSP 40/70 particles.....	68
Figure 4.29	Image of HSP 40/70 #2 particles.....	69
Figure 4.30	Cross-sectional SEM of SS316L in HSP 40/70 particles.....	71
Figure 4.31	Cross-sectional SEM of IN740H in HSP 40/70 particles.....	72
Figure 4.32	Cross-sectional SEM of HAY230 in WED 430 particles.....	72
Figure 4.33	Chemical composition of cross-sectional SEM of HAY230.....	73
Figure 4.34	Reflectance of HSP 40/70 particles between two different HT tests.....	74
Figure 4.35	Leica microscope image of HSP 40/70 untested particles.....	75
Figure 4.36	Image of same particles in Figure 4.35 after omitting particles.....	75

Figure 4.37	Outline of Figure 4.36 of the particles labeled that were considered. ....	76
Figure B.1	Surface profilometry of SS316L middle surface untested. ....	105
Figure B.2	Surface profilometry of SS316L middle surface through HSP 40/70 particles. ....	105
Figure B.3	Surface profilometry of SS316L middle surface through MAX HD 35 particles. ....	106
Figure B.4	Surface profilometry of SS316L middle surface through WED 430 particles. ....	106

## LIST OF ABBREVIATIONS

BE	Brayton Energy
CSP	Concentrated solar power
DOE	The Department of Energy
HAY230	Haynes 230 material
HSP 40/70	CARBOBEAD HSP 40/70 particles
HT	High temperature
HTM	Heat transfer medium
IN740H	Inconel 740H material
LT	Low temperature
MAX HD 35	CARBOBEAD MAX HD 35 particles
NREL	National Renewable Energy Laboratory
OO	Oxidation only
PV	Photovoltaics
SNL	Sandia National Laboratories
SEM	Scanning electron microscope
SS316H	Stainless steel 316H material
SS316L	Stainless steel 316L material
TES	Thermal energy storage
WED 430	Silica quartz Wedload 430 particles



## CHAPTER ONE: INTRODUCTION

### 1.1 Motivation

Throughout history, energy consumption has increased as technology has advanced. As the world has continually depleted its nonrenewable resources, cutting edge research has been focused towards different renewable alternatives to help power our ever-changing world. There are many different types of renewable energy, including but not limited to solar, wind, biomass, and hydro energy.

Solar energy has great potential, as the amount of solar energy that can be used on Earth is over 200 times the total annual commercial energy usage [1]. Solar energy is affordable and accessible in all areas of the United States. Potential capacity in solar power has grown from 0.34 gigawatts (GW) in 2008 to around 97.2 GW today [2]. To put that in perspective, 97.2 GW can power around 18 million American homes. Despite all its potential, solar energy only provides around 3% of the energy used in the United States. In the past decade, solar has taken off and substantial investments have been put into research on harvesting and storing solar energy. The main ways of generating and storing solar energy include solar photovoltaics (PV) and concentrated solar power (CSP) plants. Solar PV panel costs has decreased almost 70% while the costs of CSP plant electricity decreased 50% in the past 10 years. Projections show that CSP plants have the potential of providing “158 GW of power to the US by 2050” [2]. The Department of Energy (DOE) launched the SunShot Initiative in 2011. Their goal was to make solar energy cost competitive to other sources of electricity. One of their big focuses was to improve CSP plants.

## 1.2 Concentrated Solar Power Systems

Concentrated solar power (CSP) is a type of solar energy. It generates power by using mirrors (heliostats) to concentrate sunlight onto a receiver. Inside the receiver, the heat from the concentrated sunlight is transferred into a heat transfer medium (HTM). The heat, or thermal energy, is then used to generate electricity by spinning a turbine or powering an engine. The HTM then gets cycled and the process starts over again. There are different types of CSP systems; parabolic trough, central receiver, linear Fresnel reflector, and parabolic dish. Figure 1.1 shows the central receiver system process to get electricity from sunlight [3]. The central receiver system is large, with an electric power capacity of 10 Megawatts (MW) and above. There is often a high initial cost due to its size but it can utilize a large number of heliostats.

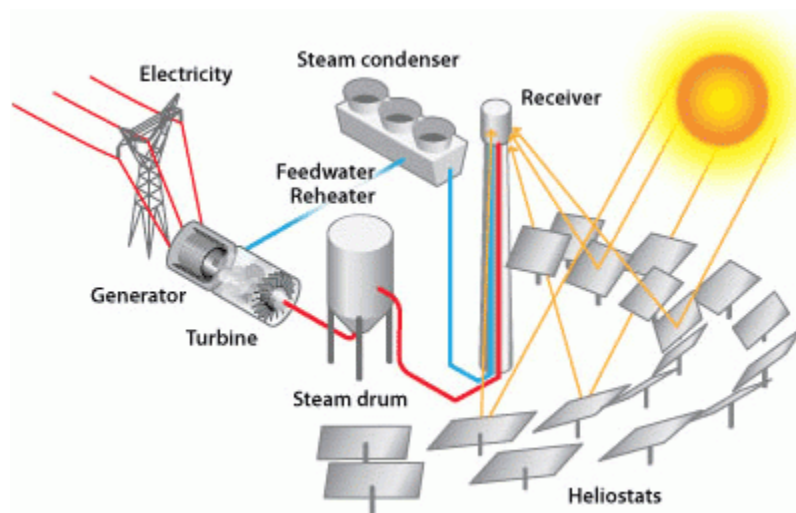


**Figure 1.1 Central receiver CSP system converting sunlight into electricity.**

The HTM in the receiver is important, as the CSP plant performance is limited by the upper temperature of the HTM. Often, nitrate molten salts are used as the HTM in CSP systems. The problem is that operating temperature of this HTM has a maximum temperature of around 565°C before becoming corrosive and unstable [4]. Additionally,

nitrate molten salt has a high freezing point of around 220°C, which makes storage difficult. Power output is very important in CSP systems and is dependent on the maximum operating temperature. The use of solid particles has the potential to have high performance at temperatures up to 1000°C [5]. To meet the goals of the SunShot Initiative, operating temperatures must be greater than 700°C. Temperatures above 700°C requires a durable HTM.

Calderon's research showed that solid particles are beneficial because they have high solar absorption rates, are more durable than other HTMs, and can be heated to temperatures greater than 1000°C, which increases the thermal-to-electric efficiency and allows an increase in energy storage [6]. One huge positive is that particles can be used both as the HTM and the thermal energy storage (TES) medium [7]. The particles can absorb the energy from the sun and can also store the heat until it is ready to be used and converted into electricity. Not only can the particles be held at higher temperatures than what is currently used, they also do not freeze.

The DOE has determined to follow the falling particle receiver route and has allotted money to growing this type of infrastructure. The focus of the research done at Boise State University can be applied to falling particle receivers, as shown in Figure 1.2 [8]. In this type of system, particles are heated by a directed beam of sunlight as they fall due to gravity. The heated solid particles are then stored in an insulated tank for later use or are then used to heat a secondary fluid [7]. This fluid is used in the power cycle, which gets the energy converted to electricity. The falling particle receiver has scalability from 10 MW to 100 MW.

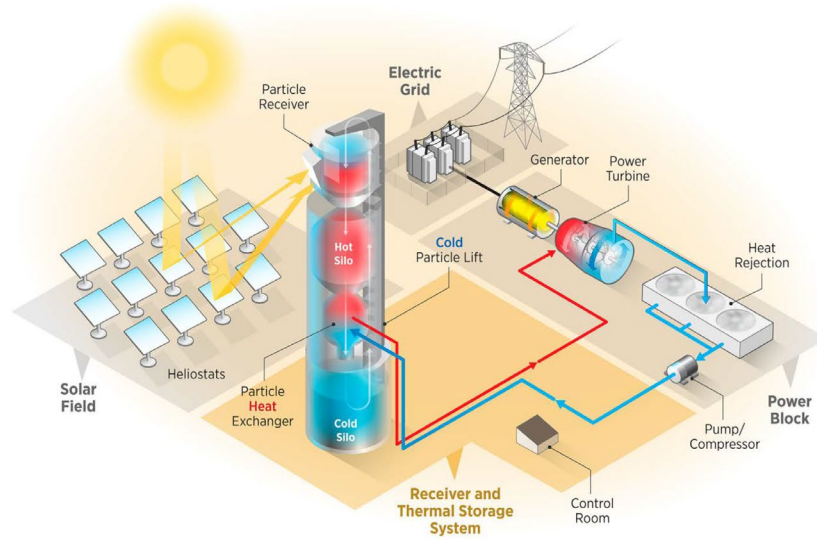


**Figure 1.2 Sketch of a falling particle receiver CSP system.**

To better understand what is happening, it is important to understand the properties and durability of the components being used in the CSP plant receiver. Running the CSP system at high temperatures has a lot of benefits but it also introduces the possibility of erosion. Understanding the potential degradation of both the solid particles and the receiver due to erosion is important with regards to the durability of running at high temperatures. Erosion in falling particle receivers can be categorized into three types of erosion: abrasion, attrition, and impact. Abrasion erosion occurs from solid particle and material contact. This happens when the solid particles fall and hit the sides of the receiver. Attrition erosion occurs when solid particles rub against each other, found when the solid particles fall and hit each other. Impact erosion occurs when the falling particles hit the bottom of the receiver before being stored in an insulated tank. The focus of this paper is on abrasion erosion.

### **1.3 Research Goals**

The goals from the DOE has led the research of this project, although the research is unique enough and can be applied to additional high temperature interactions. The goal of this thesis was to have a comprehensive understanding of material degradation due to erosion to determine durability in a CSP system at high temperatures. To fulfill this goal, an apparatus was designed and built to simulate the abrasion erosion found in CSP receivers- high temperature and low velocity.

## CHAPTER TWO: BACKGROUND AND LITERATURE REVIEW

### 2.1 Introduction

Solar energy has great potential, as the sun has an abundant amount of unutilized energy. CSP plants can harness the energy of the sun. Nitrate molten salt is commonly used as the HTM but it has been found that running CSP plants at high temperatures can increase thermal efficiency in heat transfer and reduce thermal energy storage costs. To run these CSP plants at high temperatures that can reach greater than 1000°C, solid particles are being researched, as they can be both the HTM and TES and do not freeze, unlike nitrate molten salt. With running at high temperatures, erosion also occurs. This chapter will include what causes erosion, oxidation at high temperatures, and previous research regarding abrasion wear and oxidation.

### 2.2 Factors due to Abrasion Erosion

Erosion is an important factor in many different applications. It occurs in numerous instances and is often referenced in agriculture and oil and gas industries as erosion can easily cause damage and failure to facilities. Abrasion erosion occurs when solid particles rub against a material, most commonly a metal. This type of interaction can be found in falling particle receivers when the particles flow down the receiver and hit the sides of the receiver walls. Abrasion erosion can be compared to sandpaper rubbing against a block of wood. As the sandpaper continues to rub against the block of wood, both the block of wood and the sand paper begins to get smoother. Just like different sandpaper grits and different types of wood combinations results in different amounts of smoothness overtime, different

types of particle and material combinations also results in different erosion rates over a period of time. The erosion rate due to abrasion wear can depend on velocity, the properties of particles, including shape, size, and hardness, the properties of the material, including hardness, brittleness, and ductility, and temperature.

Understanding what can affect the erosion process can help determine what combination of particles and receiver materials would work best for CSP plants. In addition, understanding the erosion lifetime can help determine when maintenance needs to be completed to help improve human efficiency.

#### Erosion due to Velocity

One of the earlier studies of erosion due to solid particles was in the 1960s by Finnie. Annealed SAE 1020 steel specimens were hit by silicon carbide grains at an angle of 20°. Initial work concluded as velocity increased, the rate of erosion increased, as shown in Figure 2.1 [9].

Yabuki tested particles on metallic materials. It was found that as the velocity of the metal decreased, the particles striking the metal did not skid as much. The reduced amount of skidding decreased the damage done on the metal [10].

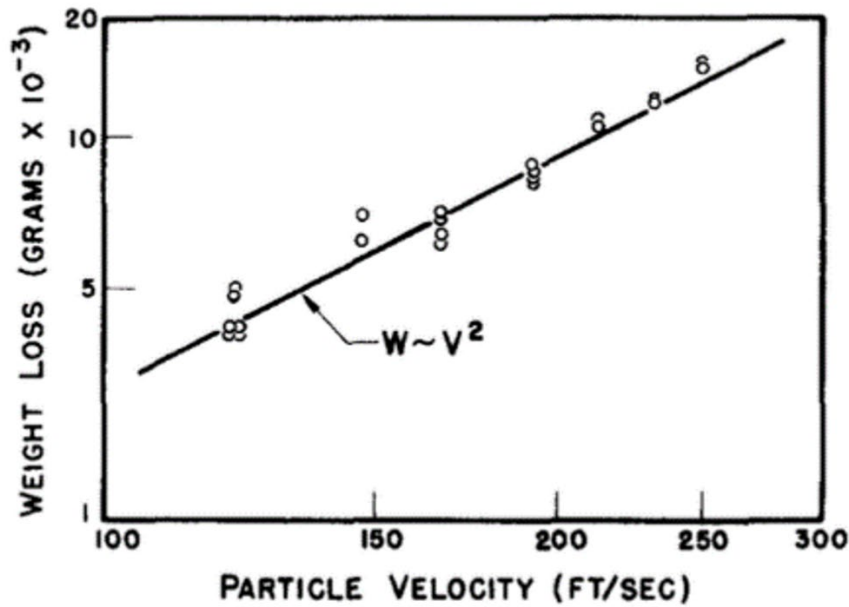


**Figure 2.1** Effect of the velocity of silicon particles on steel metal at an angle of 20° [9].

#### Erosion due to Particle Shape and Size

It has been found that both a particle's shape and size have an impact on the rate of erosion on a material. Lin created an experiment to test different particle sizes and shapes, along with different flow rates to determine their effects on erosion [11]. Silica sand particle sizes included 75, 150, 300, and 600 $\mu$ m. Particle shape was determined by the particle sharpness factor, making the sharper sand, referenced as angular, found in 75 $\mu$ m and 600 $\mu$ m particles while less sharp sand was considered semi-rounded, and found in 150 $\mu$ m and 300 $\mu$ m particles. The tests ran at room temperature. The erosion ratio and sharpness factor were used to find the erosion rate based on the shape of the particle where  $ER$  is the erosion rate and  $F_s$  is the sharpness factor of the sand.

$$ER_{shape} = \frac{ER}{F_s} \quad (2.1)$$

Lin found that the erosion ratio increased as the particle size increased in Figure 2.2.

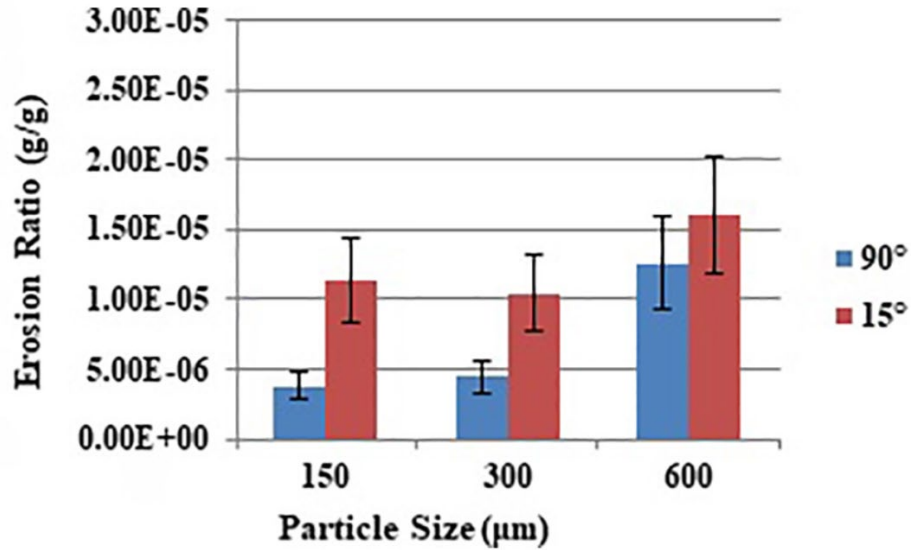


Figure 2.2 Erosion rate based on particle size. Edited from [11].

Lin compared the results of 300µm to a previous test by Li. Lin's particles had a shape factor of 1.0 and Li's particles had a shape factor of 0.53. This means that Lin's particles were more round while Li's particles were angular. The sharper particles Li used concluded that angular particles had a greater effect on the erosion ratio, as shown in Figure 2.3.

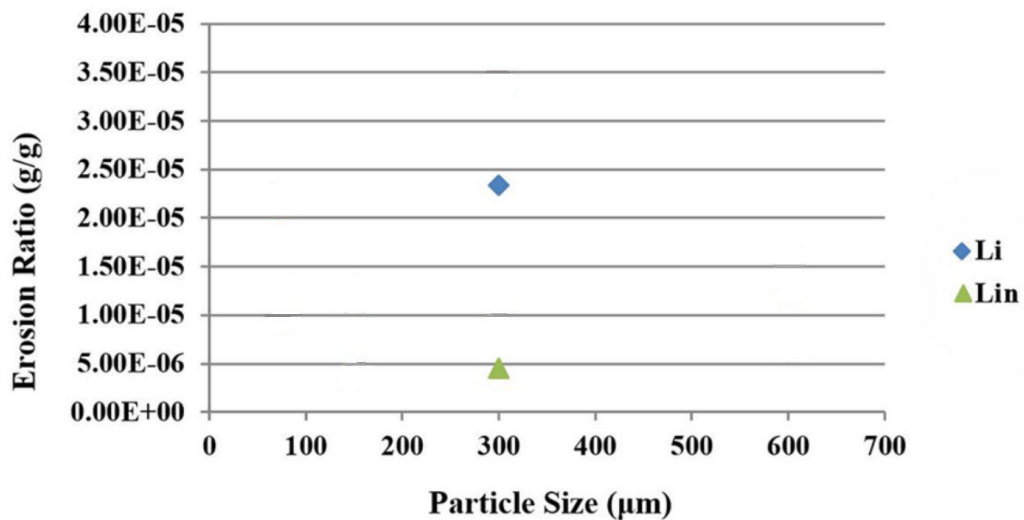
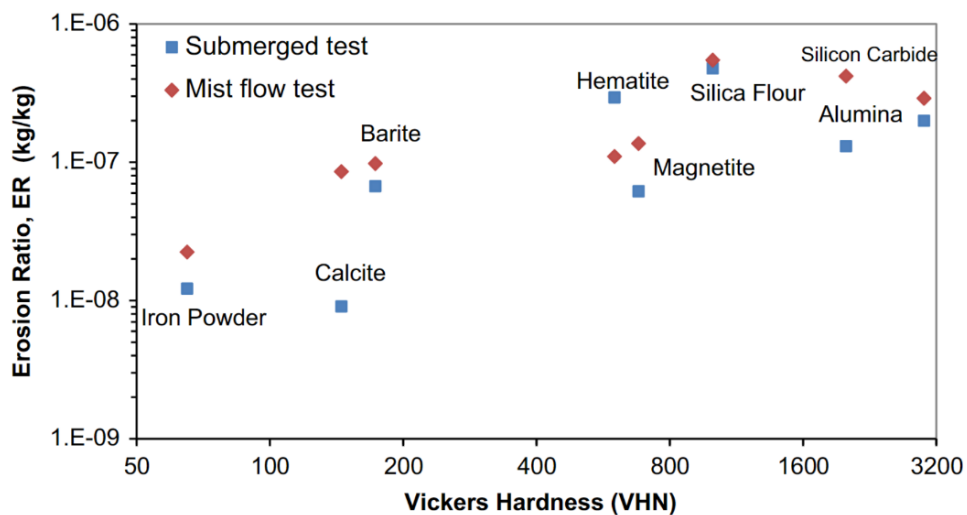


Figure 2.3 Comparing erosion rate of Li's angular particles and Lin's rounded particles. Edited from [11].

### Erosion due to Particle and Material Hardness/Ductility

Erosion occurs when particles connect with materials and an important factor is the hardness of the particles and the material. Arabnejad studied how particle hardness effects the erosion in stainless steel [12]. Two test apparatuses were built, one where the particles were submerged in a liquid jet and a second where particles were in a mist flow. Both continuously hit a stainless steel surface. The results, found in Figure 2.4, concluded that there were higher mass losses (and erosion ratios) from particles that ranked higher on the Vickers Hardness scale.

Divakar tested stainless steel with different surface hardness values to prove their effect on erosion [13]. The hardness of the steel was based on cold rolling and case hardening. This test determined that the steel with higher hardness values were more resistant to erosion and did not lose as much mass.



**Figure 2.4 Erosion ratio of particles compared to their hardness [12].**

Wilson created an impeller wear apparatus to test impact wear and abrasion wear at the same time [14]. Impeller paddles rotated in a cylindrical drum. The paddles held the

specimens and the drum rotated particles. The large drum holding the particles rotate at 45 rotations per minute (rpm) and the paddles rotate at 620 rpm (or about 6 m/s). They both rotate in the same direction. Tests ran at room temperature for 5 hours with stainless steel 304 and different particles, including high-silica quartzite, granitic ore, and limestone. The specimens were sanded down before being tested. The volume loss was found for the steel through different particles and is shown in Figure 2.5. The conclusion was that materials wore down over time at different rates after exposure to particles. It was found that the impeller-drum method produced realistic wear studies.

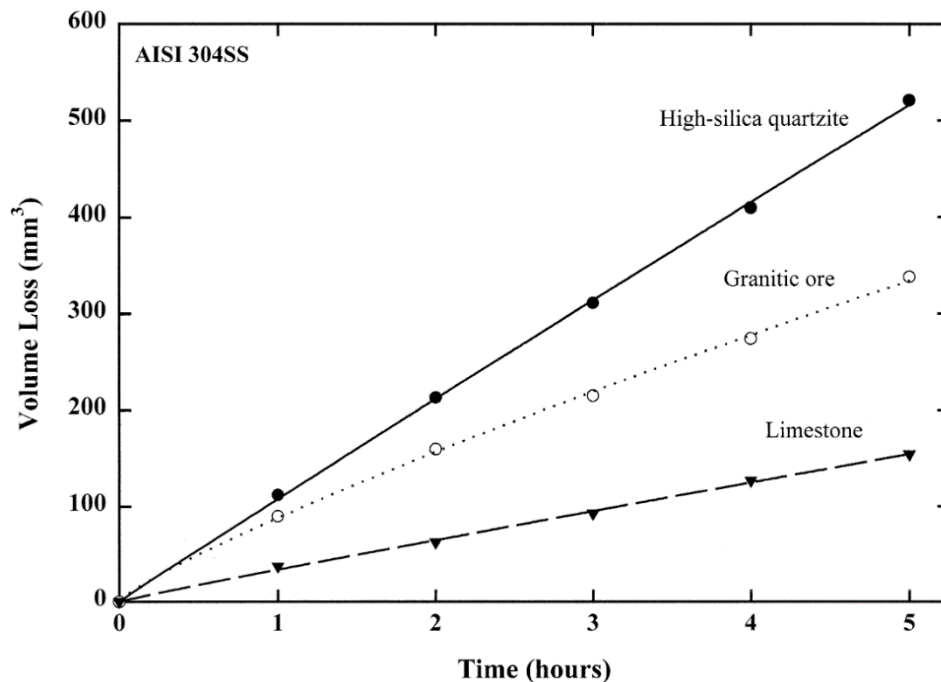


**Figure 2.5** Volume loss of stainless steel 304 through different particle [14].

### 2.3 Oxidation and Erosion at High Temperatures

It is important to understand the particle and material properties to know how they affect erosion. These tests so far are not run at high temperature. Running at high temperatures brings in oxidation. Both erosion and oxidation will occur simultaneously but

knowing how they interact together and separately is important. Oxidation occurs when there is a change in chemical composition due to the addition of oxygen and has a large impact on the erosion rate of particles and materials. Understanding oxidation is important because it can reduce wear rates of materials and particles. Oxidation has been studied as it is a real-world problem in a majority of fields such as gas and oil, marine, and chemical and power generation. Oxidation is a complicated subject, as it can both cause wear on materials and also create a protective oxide layer.

### Oxidation and Wear Basics

Wear is often influenced by heat, either by friction or externally applied. This often results in oxidation, which affects the wear rate. Stott discussed how oxidation plays a role in the wear in alloys via sliding wear [15]. Mild steel was used and it was found that in temperatures up to 570°C, the steel forms a layer of iron oxide. This refers to the barrier layer and is used to decrease the amount of wear over a longer period of time. It was found that the thickening rate on the layer of oxide depended on factors including temperature, oxygen pressure, and structure of the initial oxides. When looking at steel, the oxide usually continues to grow until it reaches a thickness of about 10µm. After that, wear occurs due to the removal of oxide, mostly due to frictional heat. It was also noted that oxides would continue to grow, even after a layer has been taken off. Figure 2.6 shows the oxide building up before it breaks off. Once it breaks off, Figure 2.7 shows how a new layer of oxide then begins to grow.

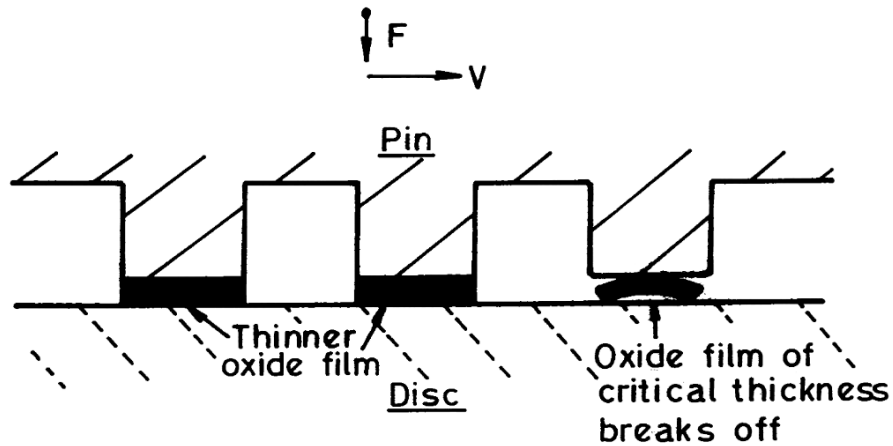


**Figure 2.6** Sketch of oxidation layer building up on a surface before breaking off [15].

Stott follows up with another article on sliding wear of materials at high temperature [16]. The experiment was conducted at multiple temperatures between 20 and 800°C. It was concluded that over long periods of time, a hardened layer of oxidation built up on the surface which ultimately decreased the amount of wear at higher temperatures. Unfortunately, each of these tests were only ran for around 27 hours, which is not a comparable amount of run time in CSP plants.

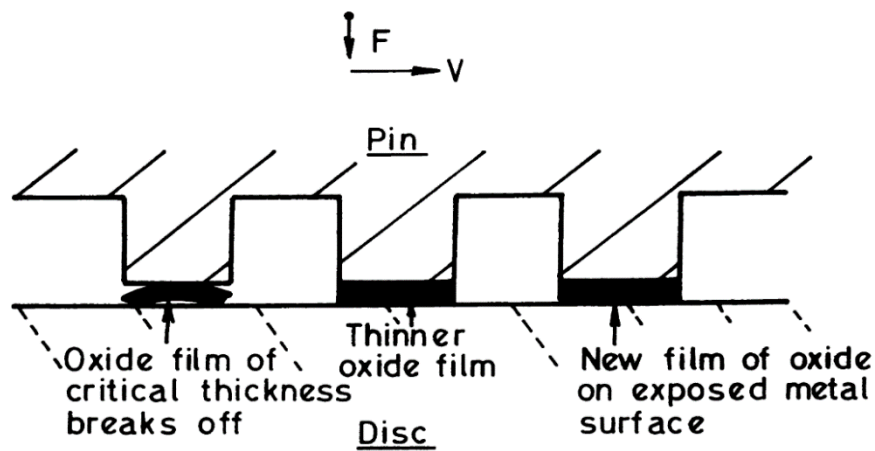


**Figure 2.7** Sketch of oxide breaking off and a new oxidation layer forming on the surface [15].

### Oxidation in Stainless Steel

Recently, testing was completed to view oxidation on stainless steel over a long exposure time. Huang observed oxidation of stainless steel 316L (SS316L) at 400, 600, and 800°C for exposure times of 100, 500, and 1000 hours [17]. SS316L was used over other stainless steels because of the additional ~3% Molybdenum, which made the material more corrosive resistant. The specimen used had the dimensions of 20x10x3mm<sup>3</sup> (0.8x0.4x0.12in<sup>3</sup>). The tests ran the full number of hours desired before cooling down to room temperature.

Huang noticed that spalling occurred. Spalling occurs when the surface of a metal fails and breaks down into flakes. Two tests ran, one where the material was not messed with and another where the spalling was taken off. Figure 2.8 shows the results of SS316L weight gain when the spalling was not messed with while Figure 2.9 shows the results when the spalling layers were taken off before each measurement. Figure 2.8 showed a weight gain in a parabolic trend. Figure 2.9 showed an initial increase before a decrease. The initial increase shows that there is oxidation building up on the surface but not enough to result in spalling. The decrease occurred after enough spalling was built up and it was removeable.

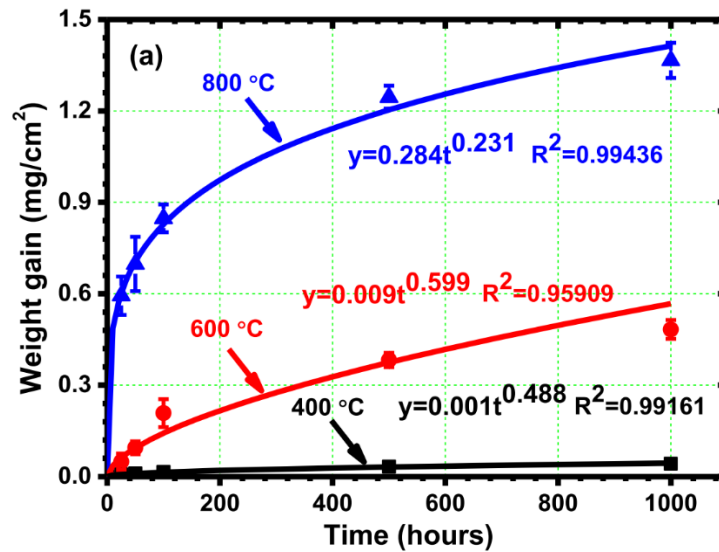


**Figure 2.8** Testing of SS316L exposed to different temperatures over a period of time with no spalling removal [17].

It was concluded through analysis that multiple oxidation layers consisted of different elements based on the temperature the experiment was being ran. Huang also concluded that Figure 2.9 would never reach an equilibrium point. This is because there was continual spalling, even at high temperature for long periods of time.

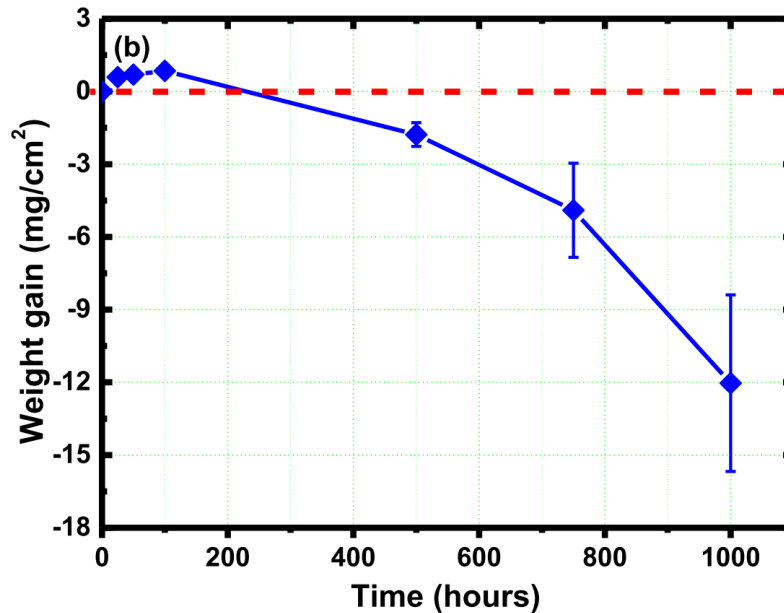


**Figure 2.9** Testing of SS316L exposed to 800°C over a period of time while removing spalling [17].

#### 2.4 Testing of Abrasion Erosion and its Application to CSP Plants

There have been experiments regarding the use of solid particles as the HTM and the TES as they relate to CSP plants and particle-based receivers. The first paper shows a comparison of oxidation and erosion and the second paper has an experiment that is similar to the desired research.

##### Abrasion Wear and Oxidation Experiment

Antonov and Hussainova created a two-chamber experimental set up to test abrasion and oxidation at high temperatures [18]. The two chambers let the effects of wear and oxidation be seen by themselves and together to view if they affect each other. The samples are mounted on a disk and rotated through particles, as shown in Figure 2.10. The specimen's surface, Figure 2.11, had different sides which allowed some sides to experience wear while other sides did not. This test was running at different temperatures ranging from 20 to 1000°C but only ran 5 hours due to the wear found on the bearings and

disks in the apparatus. The equation used to calculate wear at high temperatures is equations 2.2 and 2.3.

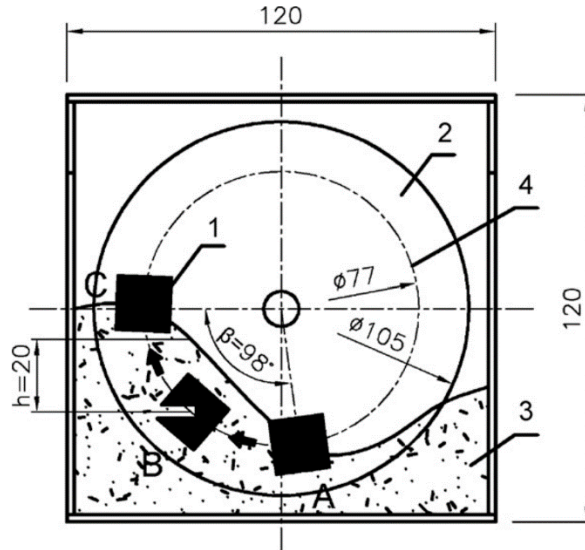


**Figure 2.10** Sketch of apparatus showing specimen moving through particles. Units are in mm [18].

$$W_{AO} = \frac{W - (A_{OO}K_O t_{AO})}{A_{AO}t_{AO}} \quad (2.2)$$

Where

$$K_O = \frac{W_O}{A_O t_O} \quad (2.3)$$

$A_O$  refers to the area of the sample exposed to oxidation,  $A_{OO}$  is the area of the sample that does not undergo wear, and  $A_{AO}$  is the area of the sample that is subjected to wear.  $K_O$  is the oxidation rate,  $t_O$  is the duration of the oxidation test,  $t_{AO}$  is the duration of the wear test. The ' $W$ ' symbols refers to material wastage when  $W_O$  occurs during the oxidation test,  $W$  occurs during the wear test, and  $W_{AO}$  is the wear rate.

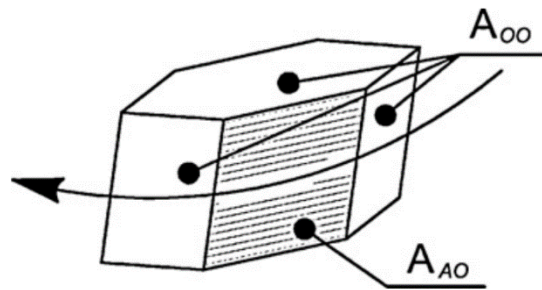


**Figure 2.11 Sample specimen and location of surfaces undergoing oxidation only ( $A_{OO}$ ) and abrasion and oxidation ( $A_{AO}$ ) [18].**

The results of this experiment and analysis showed that anything below 400°C had no signs of oxidation. There was minor oxidation at 700°C and multiple layers of oxidation at 900°C. From the nickel alloys and SS316L that was tested, it was found that there was more wear in SS316L compared to the nickel alloys. To verify the results, the synergy value was looked at. The synergy value is ratio of the abrasive wear compared to the results from corrosion. For this test, the synergy value was greater than 1, which determined that the particles created wear on the surface of the materials. This conclusion did not give specific values of wear and due to the type of experiment, they were unable to run for long durations of time, which would better simulate a CSP plant.

#### CSP Particle Receiver Experiment

Testing of alloys at high temperature and low velocity has been done before. Oxidation and erosion of potential materials and particles for CSP systems were analyzed [19]. The materials were fixed on a rotating carousel-type holder, as shown in Figure 2.12. The container was filled with particles and the carousel-type holder was fully inserted into the bed of particles with an external motor to rotate the particles at a rate of 2.8 cm/s.

The specimens were taken out every 100 hours for measurements and each experiment ran a total of 500 hours of run time. Each type of specimen was tested at four

different temperatures, ranging between 400 and 750°C. For this test, they looked at martensitic, ferritic, and austenitic alloys and used sintered-bauxite granulated particles.

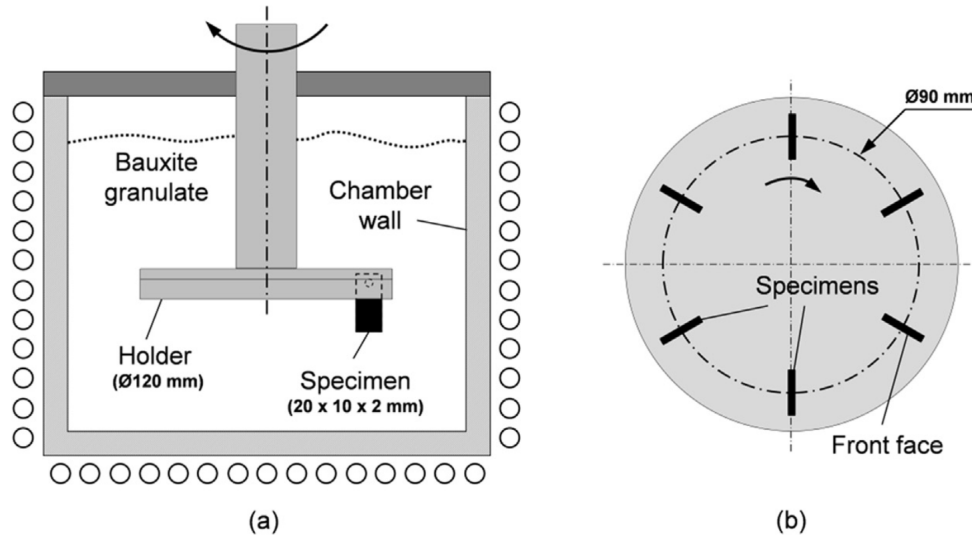


**Figure 2.12** Set up of experiment to determine abrasion wear [19].

Results showed that temperature had a substantial impact on material degradation. This is shown in Figure 2.13 for 11 wt% Cr martensitic steel VM12. The percentage of weight change increased as temperature increased. Oxidation also occurred and post-experiment scanning electron microscope (SEM) imaging showed that oxidation stayed on the specimens even after testing. The graphed results in Figure 2.13 did not consider each potential phenomenon separately. There were several simultaneous processes occurring, including material erosion, oxidation formation, and deposition of granulate material. It was concluded that the materials used might not have been the correct ones and more testing should be done using materials that had a higher hot hardness.

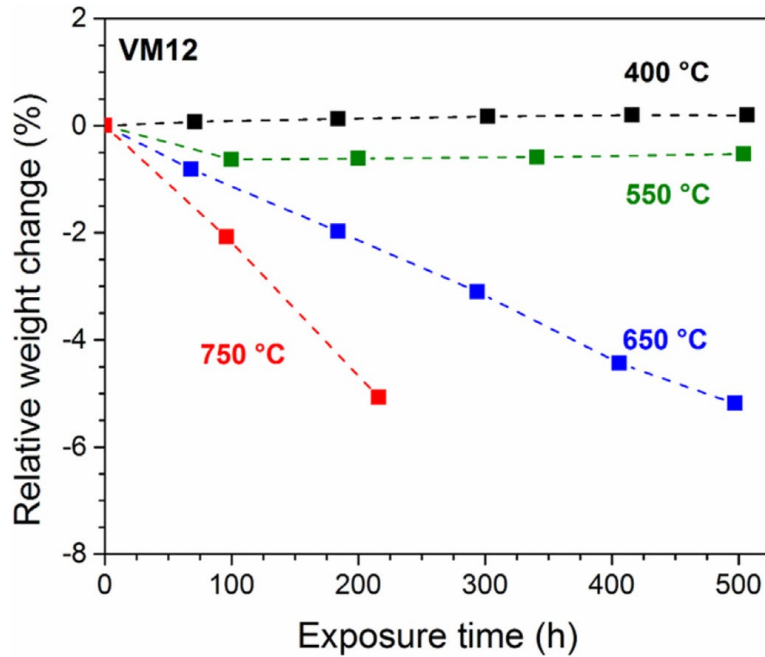


**Figure 2.13** Relative weight change vs exposure of martensitic steel VM12 [19].

This experiment is a good experiment to compare data to. The amount of test time is long and can simulate that of a CSP plant. Even though the temperature did not go higher than 750°C and speed was almost double of what is desired, predictions can be made to determine other materials that might be used. This experiment also did not use materials and particles that are currently being looked at for their abrasive wear.

## 2.5 Summary

This chapter discussed the background information needed to continue the desired research. The background previously researched has allowed a better understanding of erosion along with comparable data for testing. The main takeaways are organized below and in Table 2.1.

- Erosion due to abrasion wear is widely impacted by the properties of the particles and the properties of the materials. Understanding the influence of these factors is important because it can result in particle loss and changes in particle shape.

- Oxidation and abrasion wear can occur simultaneously.
- A majority of the experiments done in the past do not fit the criteria for CSP plants and cannot be used to evaluate the performance of the materials and particles being used for this experiment. Because of this, new experiments were developed.

A portion of this work was already published [20]. The published work included the first high temperature test with CARBOBEAD HSP 40/70 (HSP 40/70) particles and the materials of SS316L and Inconel 740H (IN740H). It had preliminary findings that are analyzed in detail in the following thesis.

**Table 2.1 Summary of research papers, the experiments, and the application.**

<b>Author</b>	<b>Material/ Particle</b>	<b>Velocity/ Speed</b>	<b>Temp of Test (°C)</b>	<b>Test Time (hours)</b>	<b>Application</b>
Antonov [18]	SS316L, sand particles	5 cm/s	400, 700, 900	5	Synergy value based on abrasive wear and corrosion
Galiullin [19]	martensitic, ferritic, and austenitic alloys, sintered- bauxite granulate	2.8 cm/s	400, 550, 650, 750	500	Relative weight change based on abrasion wear
Huang [17]	SS316L	0	400, 600, 800	100, 500, 1000	Weight gain of material affected by oxidation
Lin [11]	SS316L, silica sand	24 m/s	25	0	Particle shape and size plays an effect through erosion rate

Stott [15]	Iron & mild steels	> 5 m/s < 10 m/s	20 - 800	2.5	Sliding wear to determine layers of oxide
------------	--------------------	---------------------	----------	-----	---

## CHAPTER THREE: DESIGN AND EXPERIMENTATION

### 3.1 Introduction

From the background and research completed, it shows that there is a need for more experimental testing at high temperatures with solid particles that can be applied to CSP plants. The following chapter goes over the experimental design that was followed to simulate abrasion wear in a low velocity, high temperature CSP facility. The experiment was set up to simulate the solid particles' interaction with metal, in locations where abrasion wear is the dominant mechanism. The chapter goes into the design and details of the apparatus. It discusses the preparation needed for the specimen and how the data is tested and results are found. Additional preparation instructions for analysis are also discussed.

### 3.2 Abrasion Apparatus

To simulate the abrasion erosion in CSP plant systems, an experimental test set up was created based on the impeller-tumbler method [14]. There is a central impeller that holds and rotates “paddles” inside a container. This works well because the abrasion wear rate can be found quantitatively.

Figure 3.1 shows the schematic of the set up. There was a stationary cylindrical container that is around 4” diameter and 20” in length. The particles are placed and sat at the bottom of the cylindrical container. The specimens were cut to specific dimensions and were screwed into rods that are then attached to a shaft. The shaft has 4 drilled holes in it so the specimens and rods can be put in it. Each rod can hold two specimens. The shaft was

connected to an external motor. When the motor is turned on, the shaft rotates, which rotates the specimens in and out of the bed of particles.

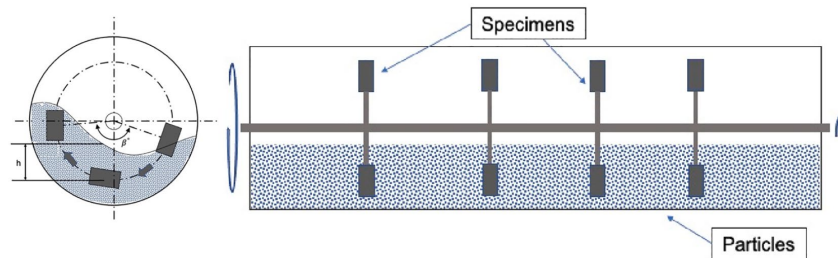


**Figure 3.1 Schematic of apparatus being used for abrasion experiment.**

Two different abrasion apparatuses were created. One apparatus was designed for a low/room temperature setting. This apparatus was made with a plastic cylinder. The other apparatus was made out of SS316L to endure the high temperature cycling. Figure 3.2 shows an image of the high temperature abrasion set up.

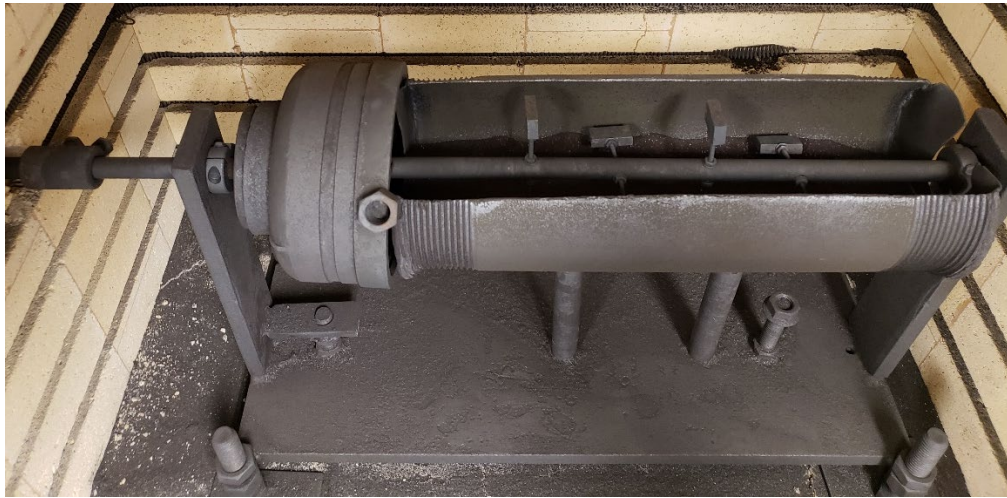


**Figure 3.2 Image of high temperature abrasion set up.**

For the high temperature set up, the experiment was placed inside a Paragon Industries kiln. To connect the shaft to the motor rod, a coupling and two screws are used, as shown on the left side of Figure 3.2. This allowed the motor to be outside of the kiln and limited

lateral and longitudinal movement of the apparatus. The motor sat on a plate and was connected to a shaft using gears, a chain, and supports. The motor was a 90-volt Leeson DC gear motor. Connected to the motor was an Eaton 512-DC-RC programmable relay. The relay was programmed so the motor would start moving at a specified time, after the kiln reached the desired temperature. The set up outside of the kiln can be seen in Figure 3.3. Collars were placed throughout the set up to help prevent lateral movement. Thermocouples were used to verify the testing temperature of the set up and the particles, based on a temperature dependent voltage.



**Figure 3.3 External Image of abrasion wear set up.**

For the low temperature set up, the motor was connected directly to the shaft. A programmable relay was not needed because the motor could start immediately since there was no preheat and kiln required.

### Speed of Rotation

The speed of the rotation was set at 1.5 cm/s to simulate a low velocity CSP plant. From there, the conversion from real time to days in a 1 MW plant operation can be found (Equation 3.1).

$$\text{Days in 1 MW Plant} = \frac{\text{hours in real time}}{\text{hours based on velocity}} \quad (3.1)$$

From this equation, it was found that running 24 hours in the kiln was equivalent to 162 days in a 1 MW CSP plant operation [21].

### 3.3 Information on Particles and Specimens

#### Specimen Material Information

Specimen materials were either given by clients, including Sandia National Laboratories (SNL), the National Renewable Energy Laboratory (NREL), and Brayton Energy (BE) or were bought through McMaster-Carr for SNL. Table 3.1 shows the materials used, their composition, some of their properties, and the client. The materials chosen were based on past research and from working with CSP developers to test materials of interest.

**Table 3.1 Information about materials used in experiments.**

<b>Material</b>	<b>Composition</b>	<b>Material Density (g/cm<sup>3</sup>)</b>	<b>Melting Point (°C)</b>	<b>Client</b>
Haynes 230	Nickel, chromium, tungsten	8.97	1,301-1,371	NREL
Inconel 740H	Nickel, chromium, cobalt	8.05	1,288-1,362	SNL
Stainless Steel 316L	Chromium, nickel	8.00	1,400	McMaster-Carr (SNL)
Stainless Steel 316H	Chromium, nickel	8.00	1,400	BE

### Particle Information

The particles were unused and were received from different clients. The bulk density and average particle size was found for each set of particles. Table 3.2 shows information on the type of particles used.

**Table 3.2 Information about particles used in experiments.**

<b>Particle</b>	<b>Material Base</b>	<b>Bulk Density (g/cm<sup>3</sup>)</b>	<b>Particle Size (<math>\mu\text{m}</math>)</b>	<b>Client</b>
CARBOBEAD HSP 40/70	Ceramic media	2.06	480	SNL
CARBOBEAD MAX HD 35	Ceramic media	2.18	580	SNL
Wedload 430	Silica quartz	1.71	477	NREL

### **3.4 Preparation**

The following section discusses the preparation needed before each experimental test is started.

#### Specimen Preparation

Table 3.3 shows the way each specimen was prepared prior to testing.

**Table 3.3 Information on how material specimens were cut and their dimensions.**

Material	Abbreviation	Cutting Device	Dimensions (in in)	Thread
Haynes 230	HAY230	EDM	1x0.5x0.5	10-32
Inconel 740H	IN740H	EDM	1x0.5x0.5	4-40
Stainless Steel 316L	SS316L	Band saw	1x0.5x0.25	4-40
Stainless Steel 316H	SS316H	EDM	1x0.5x0.3	4-40

After specimens were cut, one side was given a small divot using a punch and a hammer. This was done so that the leading edge could be differentiated from the trailing edge. The trailing edge was the surface that had the divot. Having a leading and trailing edge allowed specimen to be lined up to rotate in the same way every single time.

The specimens were drilled and tapped on a CNC mill to fit either a 4-40 threaded rod or a 10-32 threaded rod. This depended on the materials and their dimensions (Table 3.3). The specimens were soaked in ethyl alcohol to allow all the extra grease and particulates to come off so all specimens were clean. This process was done using gloves so that fingerprints would not get on them.

#### Oxidation Only Specimen Preparation

Oxidation only (OO) specimens are specimens placed in the kiln and underwent the thermal cycling but does not rotate through particles. Doing this shows the effect of rotation through particles on a specimen. This type of specimen is only applied to high temperature tests.

### Particle Preparation

There is no additional preparation for the particles. The number of particles put in the apparatus is based on the bulk density of the particles, typically between 1,300-1,500 grams.

## **3.5 Testing Instructions**

### Set Up of Experiment

To begin the test, specimens were chosen at random and ordered 1-8. The additional OO specimen was also taken when testing for high temperature. The specimens were individually placed in a petri dish one at a time and are weighed three times to establish an average mass using the Mettler Toledo balance or the Ohaus Explorer analytical balance. Both balances gave accurate results and were used based on availability. The empty petri dish was weighed after so the mass of the specimen could be calculated. After the specimens were weighed, they are placed on the apparatus in a particular order with the leading edge rotating into the particles first. The particles were then placed in the trough so that the specimens can rotate through them.

### Running the Experiments

The low temperature (LT) apparatus was ran at 25°C. The motor was turned on and the apparatus began to run immediately. The experiment was usually on for 24-150 hours before being turned off and the specimens were taken out to measure. Shop air was used to remove loose particles that may have been stuck on the specimens. The specimens were always weighed three times before being placed back into the apparatus and rotated again.

The high temperature (HT) apparatus was placed in the kiln and was turned on, running at 800°C. The kiln heats up at a rate of 400°C per hour. The programmable relay

and motor were set to turn on after two hours which aligned with when the kiln reached 800°C. The relay was programmed such that the motor would run until the predetermined time was completed and then the motor stopped as the kiln cooled down. Usually the experiment ran between 5-100 hours before being measured. The specimens were taken out of the kiln and were each measured three times.

A cycle was defined as the kiln starting at ~20°C. Then the kiln heated up to 800°C in two hours. The motor turned on and the experiment ran for a duration of time. The motor stopped and the kiln turned off after that time was completed. The kiln then took ~10 hours to cool down back to room temperature. This signified the end of one cycle.

### 3.6 Analysis Instructions

After the experiment was fully complete, multiple types of analysis was completed on the specimens and particles that were used in the experiment. Each analysis helped determine abrasion wear, erosion, and/or oxidation.

#### Measuring Abrasion Wear

For each test, the mass was recorded periodically to show the mass loss over time in the experiment. To find the abrasion wear, mass and the total surface area of the specimen was used (Equation 3.2).

$$AW \left( \frac{mg}{cm^2} \right) = \frac{m_e - m_0}{A_{SA}} \quad (3.2)$$

Where  $AW$  referred to the abrasion wear,  $m_e$  is the mass at the certain time,  $m_0$  is initial mass before testing started, and  $A_{SA}$  was the full surface area of all 6 sides. Once the abrasion wear of each specimen was found, the specimens that were of the same material were averaged.

The error for each specimen in each test was found based on the three weighed measurements and calculating the standard deviation for the sample set of the data.

### Surface Profilometry

Surface profilometry is an instrument used to find the roughness and the profile of a surface. A Wyko Veeco Optical Profilometer was used, with a repeatability of 0.01 nanometers (nm). For each test, a specimen was drawn at random after experimentation was complete. Each specimen looked at two surfaces, the middle surface and the corner of the leading edge, opposite of where the hole was drilled. The placement of where the image was taken is roughly indicated by the yellow dots on the sample in Figure 3.4.

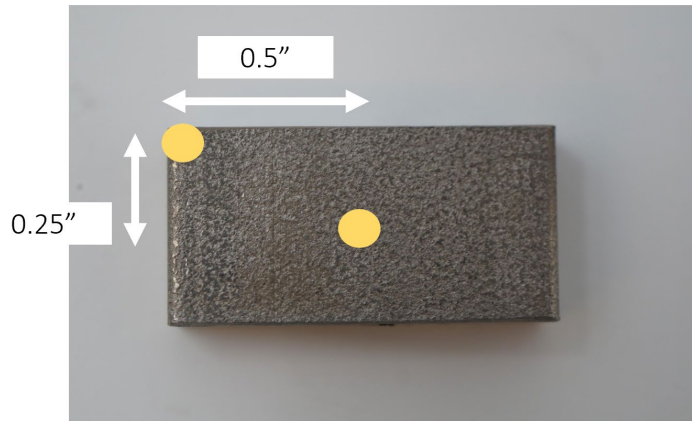


**Figure 3.4** Sample specimen of where surface profilometry was taken.

When the surface data is taken, the image is interpolated and restored to fill in the small holes that the machine did not capture (Figure 3.5). Once the data is restored, the distance taken is from the highest peak in the image to the lowest valley in the image.

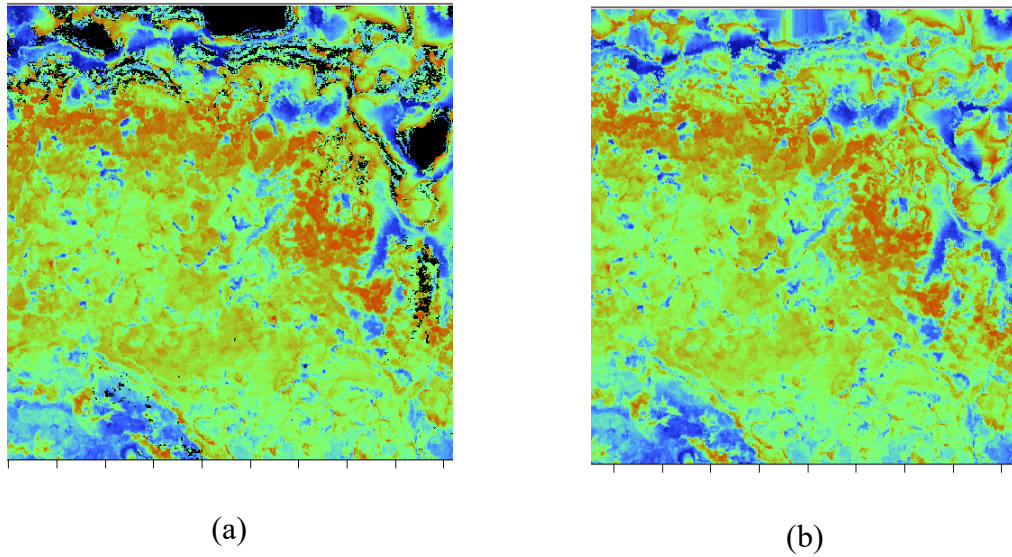


**Figure 3.5 Example of surface profilometry image (a) before and (b) after restoring data.**

#### Cross-Sectional Scanning Electron Microscope Images

Cross-sectional SEM imaging was completed on samples of randomly chosen specimen. The specimens were cut using a slow speed saw on two axes (Figure 3.6). Figure 3.7 shows a used specimen that was cut along the lines shown in Figure 3.6 The goal was to see the parallel side of the specimen so the layers developed and lost on the leading edge could be analyzed. After the saw cut the specimen, it was taken to get epoxied. Once the epoxy dried, the specimen was sanded down and then polished before being finished with a carbon coating.

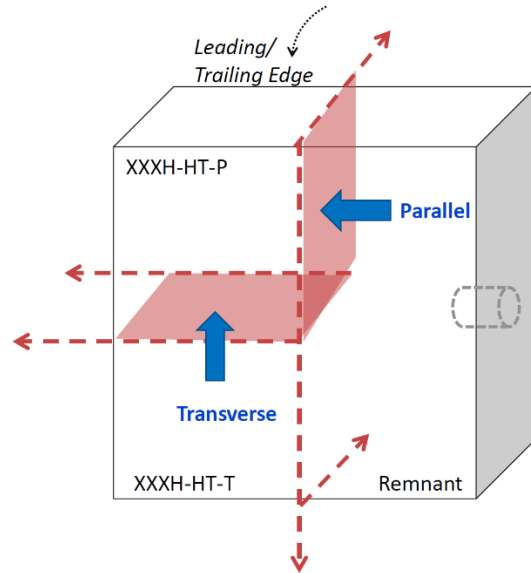


**Figure 3.6** Sketch on where the specimen was cut for cross sectional SEM, shown by the red dotted line.

The specimen was then put into the Hitachi S-3400N SEM machine. From the imaging, the layers of oxidation can be found, along with the abrasion wear on the surface. Chemical composition can also be done to show whether the surface changed chemically.

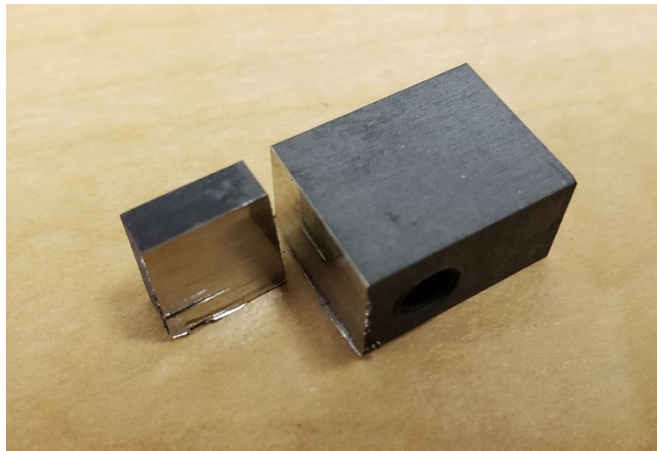


**Figure 3.7** Image of specimen cut along the parallel and transverse lines to get a sample to epoxy.

### Reflectance

The reflectance was found using a Shimadzu UV-2600 Spectrophotometer. This was used on the particles from the trough after the experiment was completed. Reflectance refers to the ratio between the energy reflected and the total energy found in a sample of particles. Showing the reflectance can help determine what is happening to the particles, and can help address oxides and additional particles found in the trough. The software program was turned on and a baseline was established. The wavelength was between 300-1400 with a slit width of 1.0 and an interval of 0.5. Particles are scooped up into the glass particle holder, rotating each scoop to get a good mixture. The reflectance was taken three times, with three different scoops of particles. The data is averaged amongst the samples.

### Optical Microscope and Particle Analysis

The particle analysis utilized a sample of particles drawn at random. The particles were stuck on a piece of paper using double sided tape before imaging with a Leica CTR6000 microscope with a 5x lens. ImageJ was used to analyze particles. Particles were analyzed for the Feret diameter, standard deviation based on the sample size, and the circularity. The averages for each of the findings were taken. Feret diameter was found by measuring the size based on a specified direction. Circularity is a percentage to show how close the particle is to a “perfect” circle. It is based on area ( $A$ ) and perimeter ( $P$ ) (Equation 3.3).

$$circularity = 4 * \pi * \left( \frac{A}{P^2} \right) \quad (3.3)$$

## CHAPTER FOUR: RESULTS AND ANALYSIS

### 4.1 Introduction

From the experiments, the mass of the specimens was noted. Abrasion wear was calculated and analyzed based on temperature, rotation, and oxidation. The HSP 40/70 particle test for SS316L was looked at in detail because the results were different from the rest of the results. Surface profilometry, cross-sectional SEM, and the specimen's chemical composition was used to study the specimens and reflectance and particle analysis was done to analyze the particles.

### 4.2 Untested Particle Analysis

The particles being used include CARBOBEAD HSP 40/70 (HSP 40/70), CARBOBEAD MAX HD 35 (MAX MD 35), and Wedload 430 (WED 430). Table 4.1 shows information on the analysis of these particles.

**Table 4.1 Information on particles using in testing.**

<b>Particle</b>	<b>Avg Particle Size (<math>\mu\text{m}</math>)</b>	<b>Standard Deviation (<math>\mu\text{m}</math>)</b>	<b>Particle Shape</b>	<b>Particle Image</b>	<b>SEM Figure</b>
HSP 40/70	480	7.061	Round	Figure 4.1	Figure 4.2
MAX HD 35	580	52.282	Circular, flat	Figure 4.3	Figure 4.4
WED 430	477	7.262	Round, Angular	Figure 4.5	Figure 4.6

Images and SEM images were taken on the untested particles. HSP 40/70 particles (Figure 4.1 and Figure 4.2) are a type of ceramic media. They have a round shape and are uniform in size.



**Figure 4.1** Image of untested HSP 40/70 particles.

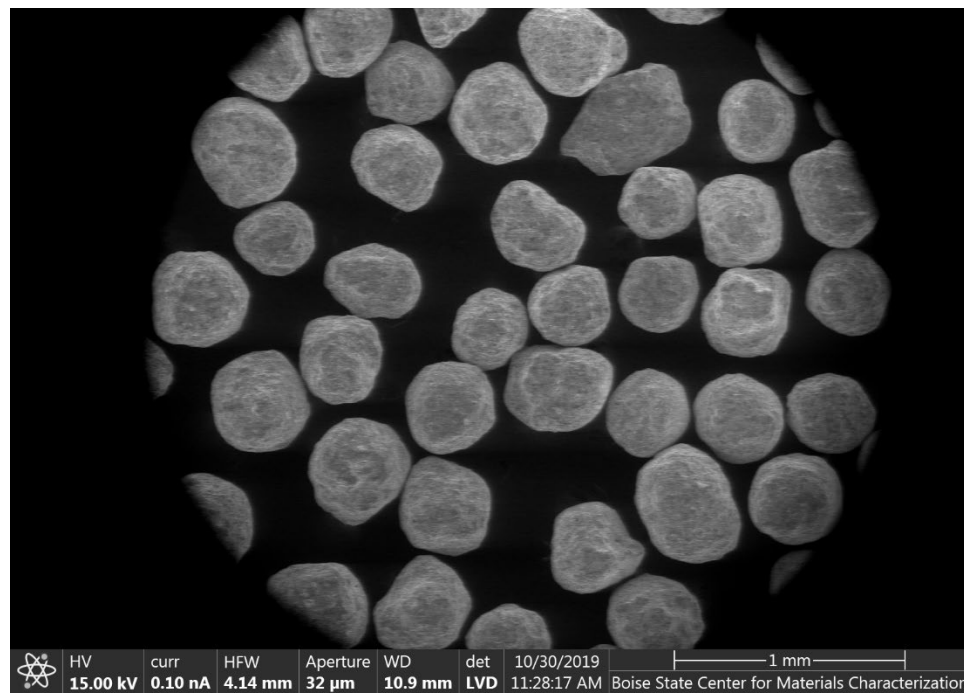


**Figure 4.2** SEM image of untested HSP 40/70 particles.

MAX HD 35 particles (Figure 4.3 and Figure 4.4) are also a ceramic media, like HSP 40/70 particles. Compared to HSP 40/70 particles, they are around 100μm bigger in size, have a smooth surface, and a uniform round shape.



**Figure 4.3** Image of untested MAX HD 35 particles.

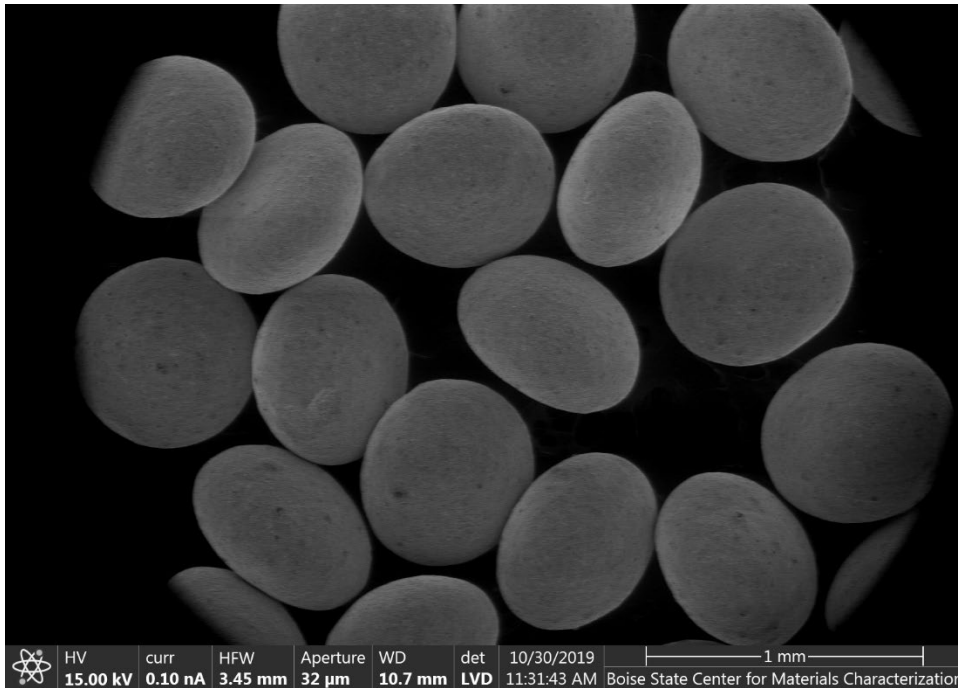


**Figure 4.4** SEM image of untested MAX HD 35 particles.

WED 430 particles (Figure 4.5 and Figure 4.6) differ from the other particles as a silica quartz media. These particles are about the size of HSP 40/70 particles but based on the SEM image, these particles are not as round in shape and also are not as uniform. Compared to the other particles, these particles are more angular and have sharper edges.



**Figure 4.5** Image of untested WED 430 particles.

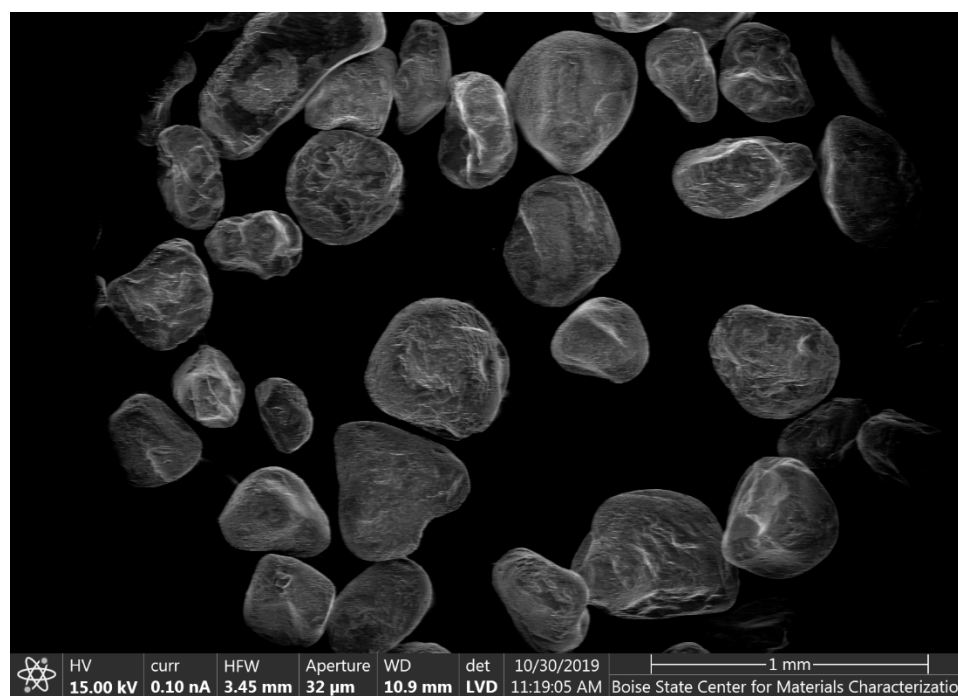


**Figure 4.6** SEM image of untested WED 430 particles.

### 4.3 Thermocouple Verification

As stated before, thermocouples were used to verify that the temperature of the kiln and the particles were at 800°C. HSP 40/70 particles were tested to confirm this. There were three total thermocouples. There was an “Ambient” thermocouple that was just outside the kiln. The “Kiln” thermocouple referred to the thermocouple that was in the kiln

but not touching any surface to get the air's temperature. The "Particles" thermocouple referred to a thermocouple that was placed in HSP 40/70 particles to see the temperature of the actual particles that the specimens were moving through. "Programmed" was what the rate the kiln was programmed to do. This can be seen in Figure 4.7.

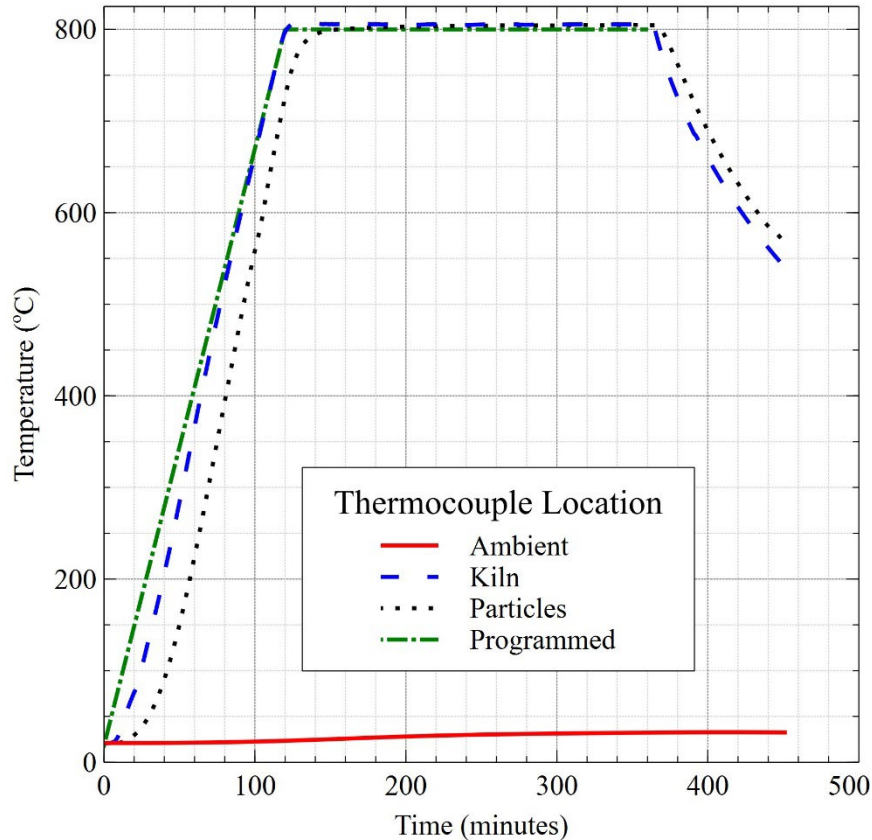


**Figure 4.7 Graph of thermocouple temperature compared to time.**

What was not predicted was the exponential slope for the thermocouple found in the particles. It was also surprising that the particles lost heat at a rate similar to the other thermocouple in the kiln. This can be shown better in Figure 4.8, a zoomed in graph of Figure 4.7. Using the thermocouples did prove that the kiln heated at a rate close to 400°C per hour and did hold at the temperature at 800°C until the test was completed.

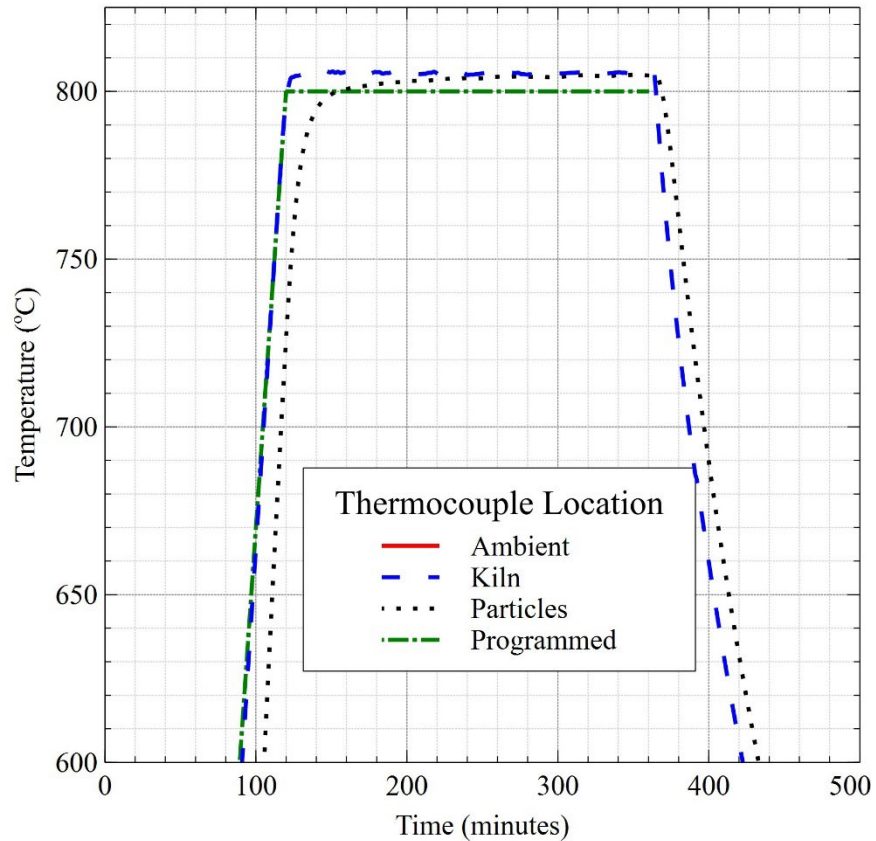


**Figure 4.8** Zoomed in image of thermocouple results found in Figure 4.7.

#### 4.4 Abrasion Wear Results

The different combinations of particles and specimens can be found on Table 4.2. The materials include Haynes 230 (HAY230), Inconel 740H (IN740H), stainless steel 316L (SS316L), and stainless steel 316H (SS316H). The particles used included HSP 40/70, MAX HD 35, WED 430. The statistics on these materials and particles can be found in the previous chapter in Table 3.1 and Table 3.2.

**Table 4.2 Combinations of the different experiments ran.**

Particle	Specimens	# of Specimens	HT Test	LT Test
HSP 40/70	SS316L	2	X	X
	IN740H	2	X	X
MAX HD 35	SS316L	2	X	X
	IN740H	2	X	X
WED 430	HAY230	8	X	X
HSP 40/70 #2	SS316L	4	X	-
WED 430	SS316L	4	X	X
	SS316H	4	X	X

The abrasion wear equation was used and the final average abrasion wear was found for each test. Table 4.3 shows the results based on each experiment and Table 4.4 shows the results based on the specimen material. Appendix A includes the mass of each specimen throughout each test.

The error of each abrasion wear test was also found. Every test, except HSP 40/70 with SS316L and IN740H test had errors of less than or equal to  $\pm 0.0006$ . This showed that results were precise and the error was not big enough to have a significant impact. The error for the HSP 40/70 test will be analyzed and explained later.

**Table 4.3 Final average abrasion wear for each experiment.**

Particle	Specimen	HT		LT	
		<i>Hours</i>	<i>Abrasion Wear (mg/cm<sup>2</sup>)</i>	<i>Hours</i>	<i>Abrasion Wear (mg/cm<sup>2</sup>)</i>
HSP 40/70	SS 316L	709	-22.0996	713	-0.2060
	IN 740H	709	-1.2358	713	-0.2329
MAX HD 35	SS 316L	741	0.4473	948	-0.1360
	IN 740H	741	0.1927	948	-0.2747
WED 430	HAY 230	871	-0.3187	1027	-0.4734
HSP 40/70 #2	SS 316L	702	-0.1601	-	-
WED 430	SS 316L	737	0.0919	790	-0.3124
	SS 316 H	737	-2.9281	790	-0.1956

**Table 4.4 Final average abrasion wear based on material specimen.**

Material Specimen	Particle	HT	LT
		<i>Abrasion Wear (mg/cm<sup>2</sup>)</i>	
SS316L	HSP 40/70	-22.0996	-0.2060
	HSP 40/70 #2	-0.1601	-
	MAX HD 35	0.4473	-0.1360
	WED 430	0.0919	-0.3124
IN740H	HSP 40/70	-1.2358	-0.2329
	MAX HD 35	0.1927	-0.2747
HAY230	WED 430	-0.3187	-0.4734
SS316H	WED 430	0.0919	-0.3124

#### Wear due to Erosion of Material

Wilson concluded that particles caused abrasion erosion over a period of time, even at room temperature [14]. Table 4.3 confirms Wilson's work with regards to LT testing. All the LT tests have a negative abrasion wear, meaning over time, it is losing mass compared to the initial mass. This concluded that erosion occurred, even with no additional form of oxidation. This proved that wear is not solely dependent on temperature but is also dependent on the interaction of specimen and particles.

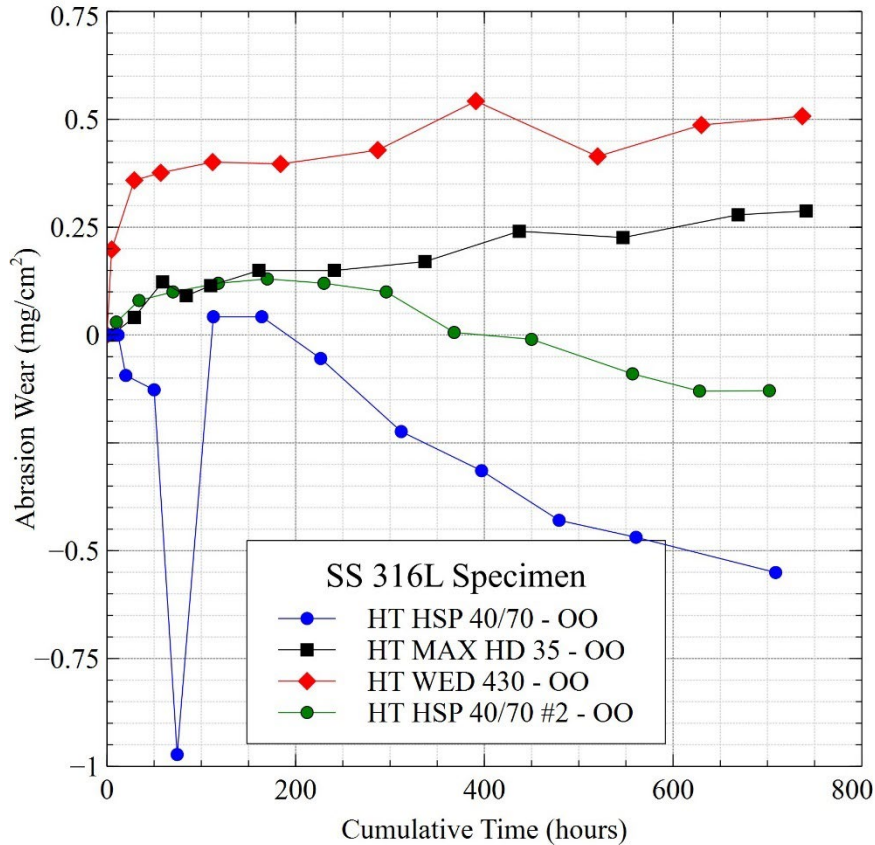
#### **4.5 Effect of Temperature on Wear**

##### High Temperature Creating Oxidation

Huang's test found oxidation of SS316L specimens [17]. The size of the specimens were different but can be used for comparison to current experiments that underwent oxidation only. Huang's one test looked at oxidation after it removed the spalling layers.

At 800°C after 1000 hours of heat exposure, Figure 2.8 showed the weight gain of the specimen was about 1.4 mg/cm<sup>2</sup> with no spalling while Figure 2.9 showed a weight gain of about -12 mg/cm<sup>2</sup> with spalling.

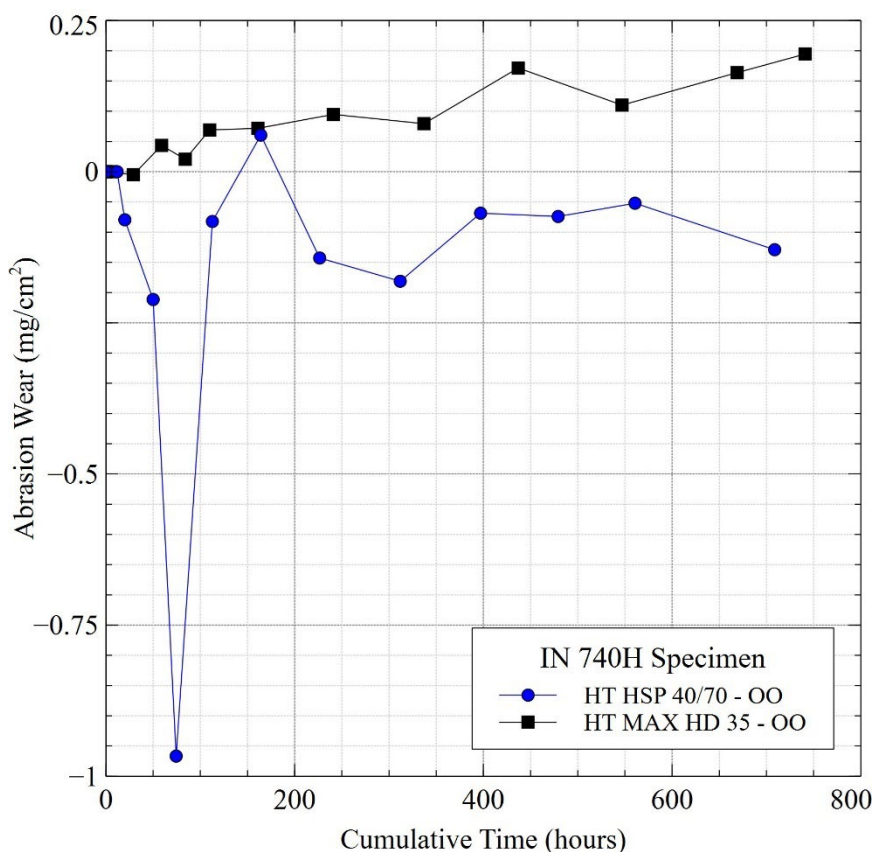
These results were a combination of Huang's work. In the experiment, spalling was noted and there were also layers of oxidation. Oxidation layers were not purposefully taken off like Huang's work but each specimen was sprayed with shop air on all side to get the loose particles and oxides off before weighing. It was not noted how each specimen was held while spraying shop air which could have an effect on how much spalling was removed. For example, if someone brushed their finger along the surface as they were spraying shop air, this could remove more spalling and oxides from the surface compared to holding the specimen by the corners. Since this was not noted, the results should be somewhere between the two weight gains of Huang's work, because some spalling was removed but not all of it.



**Figure 4.9 Abrasion wear graph of SS316L undergoing only oxidation.**

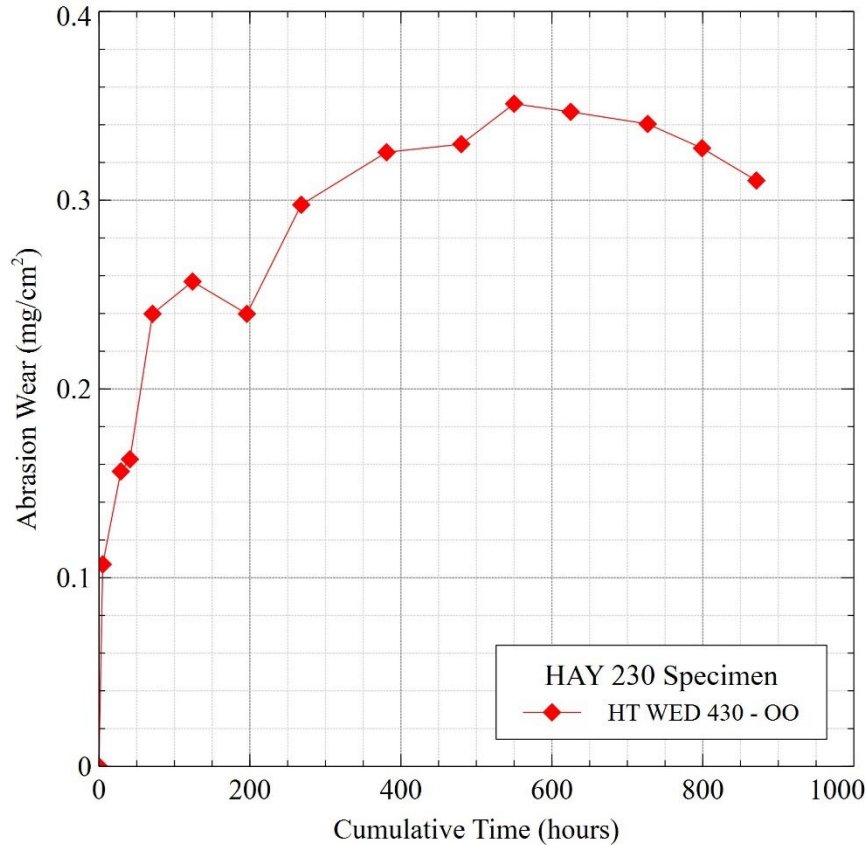
Figure 4.9 shows the results of oxidation only (OO) SS316L specimen. Even though the rotating specimens were moving through different particles, this should not have affected the OO specimens because they did not move. The conclusion was that the OO specimens should have undergone the same type of abrasion wear. Figure 4.9 shows that this did not happen and that there was a variety of abrasion wear rates in OO specimens. The SS316L specimens that sat in the back during MAX HD 35 and WED 430 particles had an increase in abrasion wear and an increase in mass. Based on previous research, these specimens gained layers of oxidation on top and were strong enough not to blow off when shop air was sprayed on the specimen. The SS316L specimens that were there during the HSP 40/70 particle tests had a decrease in mass. This showed that layers of oxides and spalling were taken out, probably by the use of shop air being sprayed on it.

Figure 4.10 looked at IN740H OO specimens. The test during HSP 40/70 particles has a decrease in abrasion wear, showing layers of oxides being removed and the test during MAX HD 35 particles had an increase in abrasion wear, so oxides stuck onto the specimen. This continues to show the variation throughout experiments.



**Figure 4.10 Abrasion wear graph of IN740H undergoing oxidation only.**

The same thing can be found in HAY230 OO where there are oxides stuck to the specimen at the beginning but then fall off at around 600 hours and SS316H OO where oxides have come off, as seen in Figure 4.11 and Figure 4.12 respectively.



**Figure 4.11 Abrasion wear graphs for HAY230 undergoing oxidation only.**

Even though there are differences in the OO specimen, whether it is increasing in mass or decreasing in mass, this shows the variability that can be found in the experiments. The specimen that had the highest increase in abrasion wear was the SS316L specimen in WED 430 particles at  $0.6 \text{ mg/cm}^2$  and the specimen with the highest decrease in abrasion wear was  $-1.7 \text{ mg/cm}^2$  with the SS316H specimen in WED 430 particles. The differences in abrasion wear is small compared to Huang's work and lays within the parameters of Huang's work, with weight gains between  $1.4$  and  $-12 \text{ mg/cm}^2$  after 1000 hours of run time.

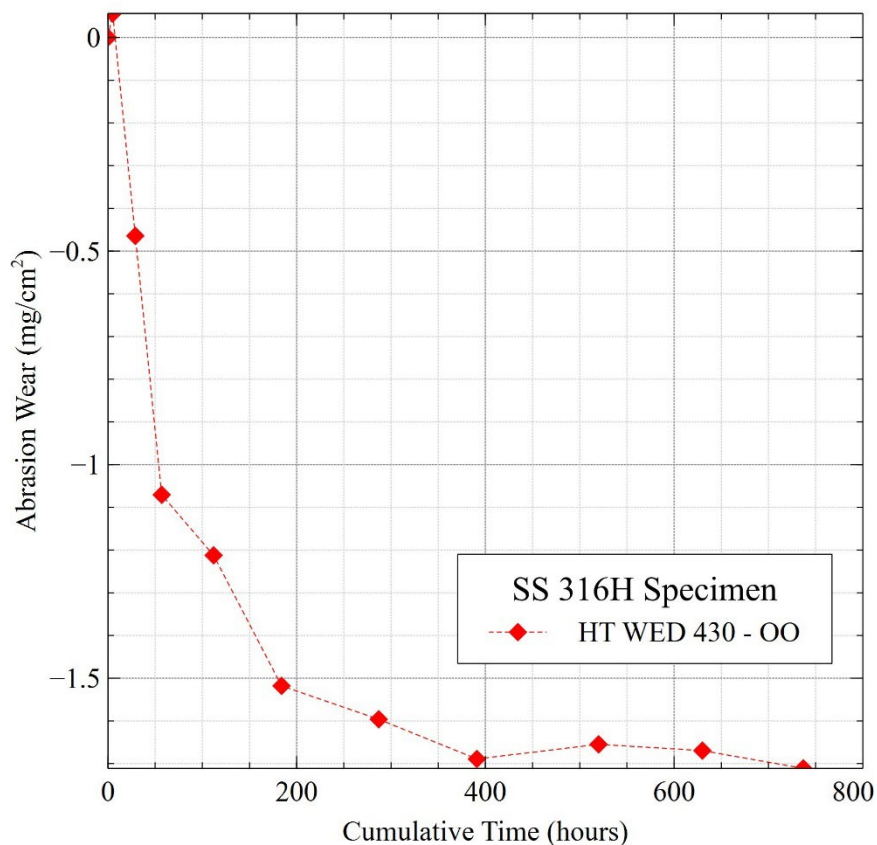


**Figure 4.12 Abrasion wear graphs for SS316H undergoing oxidation only.**

#### Abrasion Wear in HT vs LT

For SS316H (Figure 4.13) specimens, the test running at HT had a greater amount of abrasion wear than the test running at LT. The HT test had an abrasion wear of -2.93 mg/cm<sup>2</sup> over 750 hours whereas the LT test had an abrasion war of -0.27 mg/cm<sup>2</sup> over 800 hours. Based on the graph, the abrasion wear came from the first drop initially before gradually decreasing in abrasion wear. This means that there were not any oxides built up on the surface, and if there was, it either came off or was so little that it did not make a significant impact. This followed along with Antonov's conclusions regarding high temperature playing a big role in abrasion wear [18]. A greater abrasion wear means a higher weight change percentage which aligned with Galiullin's results.

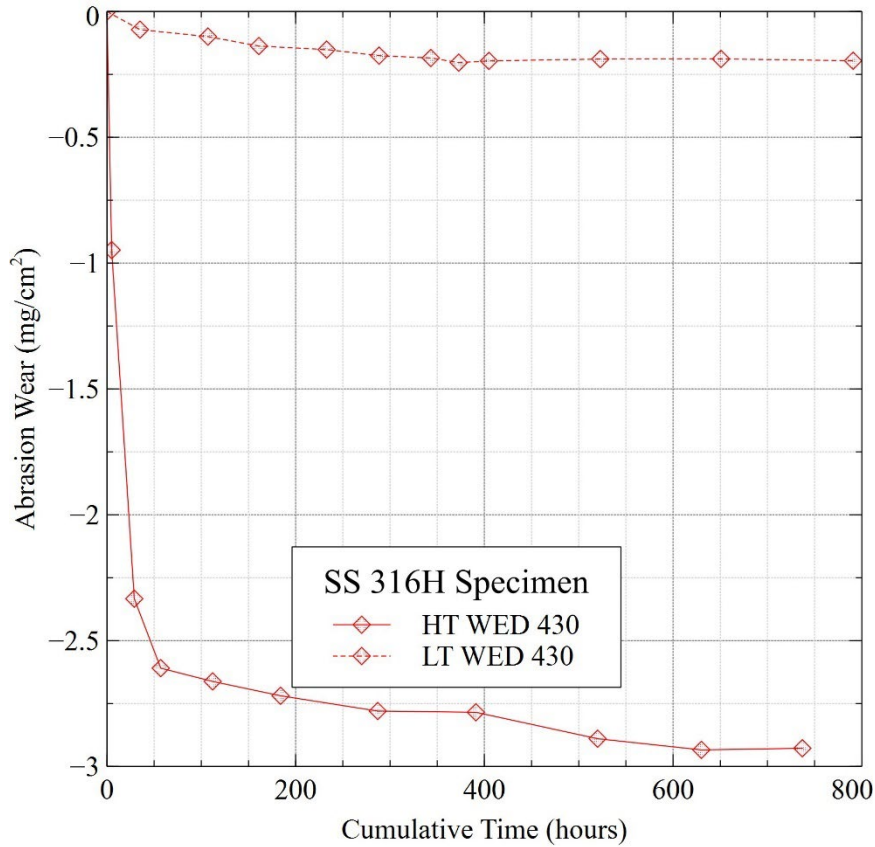


**Figure 4.13 Abrasion wear graphs of SS316H specimen effects on temperature.**

In the IN740H specimens test, for HSP 40/70 particles, the same trend was followed as the SS316H (Figure 4.13) specimens. The HT test had more abrasion wear than the LT test, with final abrasion wears of -1.2358 and -0.2329 mg/cm<sup>2</sup> respectively (Figure 4.14).

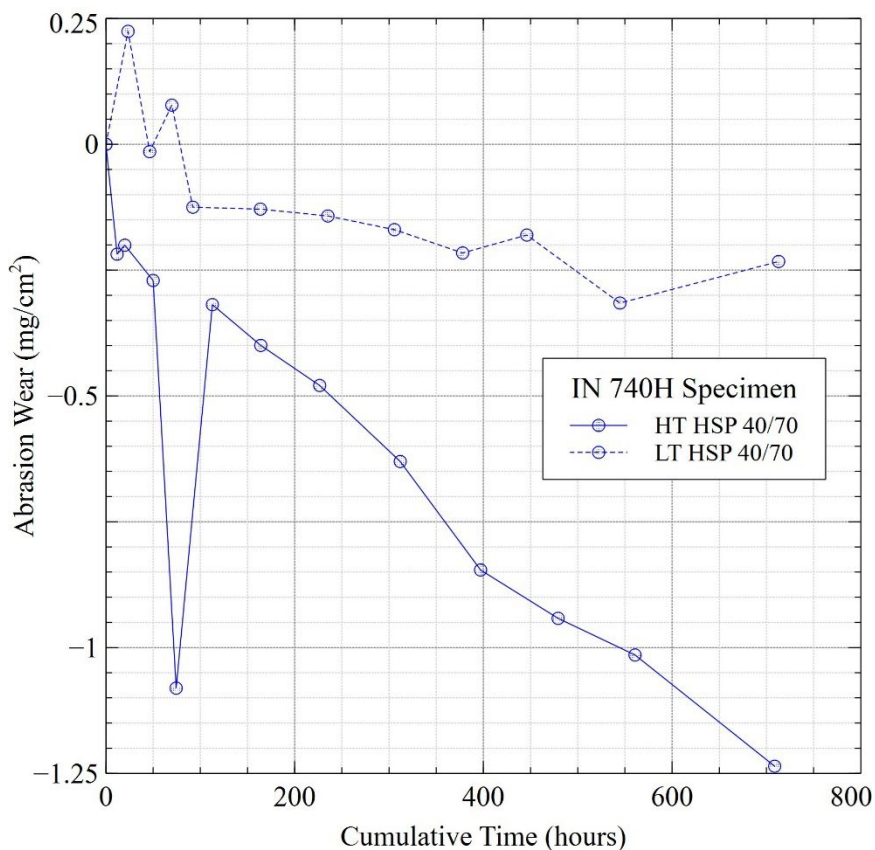


**Figure 4.14 Abrasion wear graph of IN740H specimens through HSP 40/70 particles.**

But for the IN740H specimens in MAX HD 35 particles, the abrasion wears were 0.1927 and -0.2747 mg/cm<sup>2</sup> for HT and LT respectively (Figure 4.15). The HT specimen had an initial drop in mass showing that oxidation layers did not stay on the surface. There was an increase in mass due to oxidation built up. This supports two different literary reviews. The first one was on oxidation interaction with specimen by Stott [16]. There was an oxidation built up on the specimen that never was able to shear off. The oxidation layer stayed and additional oxides build up over time. The second was with Lin's research on particle shape [11]. Through analysis, shown in Table 4.1, it was found that MAX HD 35 particles were bigger in size and smoother and rounder in shape compared to HSP 40/70

particles. The HSP 40/70 particles created more abrasion wear (Figure 4.14) as the particles were a rougher surface.

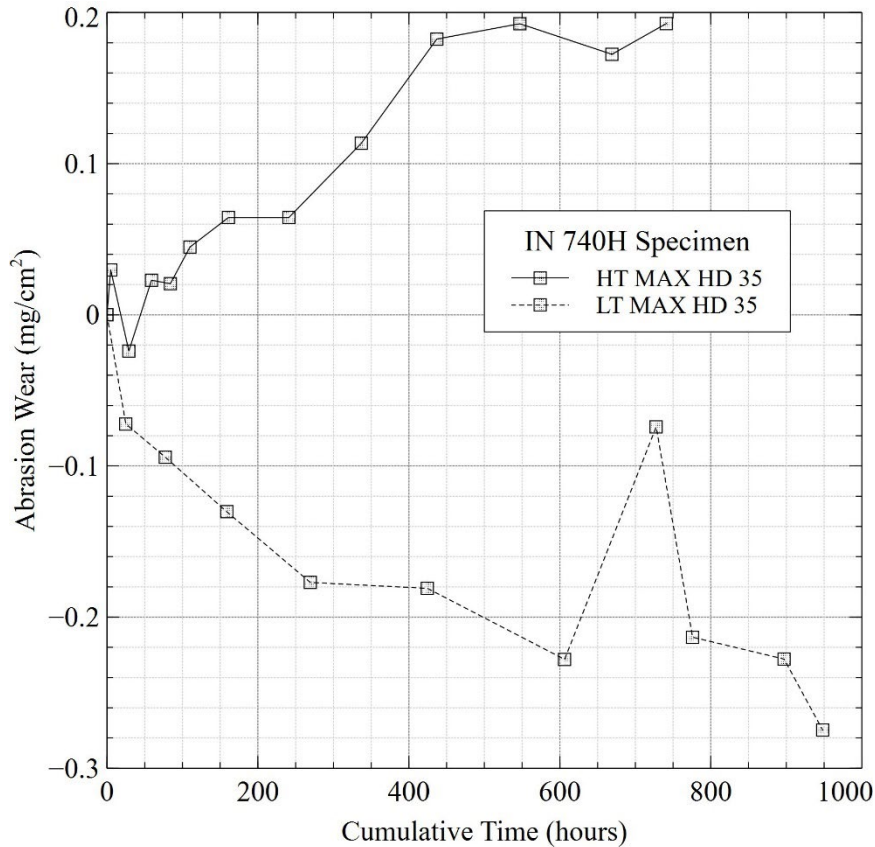


**Figure 4.15 Abrasion wear graph of IN740H specimens though MAX HD 35 particles.**

The same type of trend found in Figure 4.14 is also shown in the SS316 specimens graph for MAX HD 35 and WED 430 particles (Figure 4.16 and Figure 4.17 respectively). Lin's work was comparable with regards to how particle shape and size played a role in the wear of the material [11]. For MAX HD 35 particles, there is a mass increase to over 0.4 mg/cm<sup>2</sup> for the HT specimen, proving oxides built up on that specimens. At around 750 hours, there is a decrease in abrasion wear. Further testing is required to verify if layers of oxides were removed or if it was a measuring error and the specimens were still gaining

oxides. There was only slight wear on the LT MAX HD 35 test, showing how the large size and round shape of the particle plays less of an abrasive wear effect (Table 4.1).

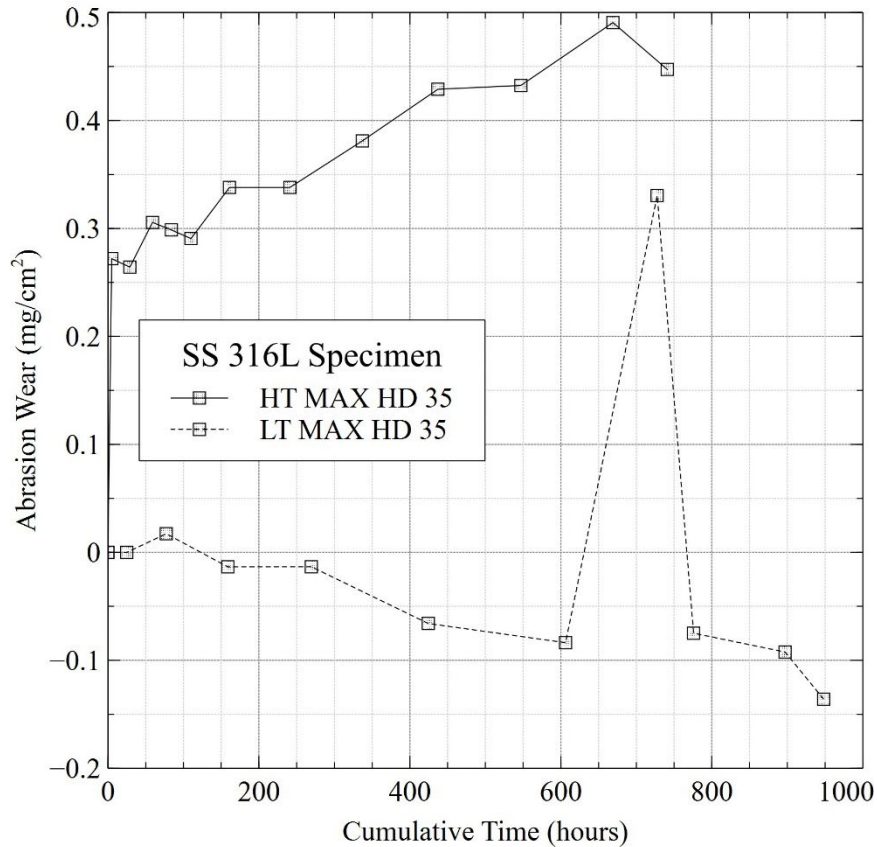


**Figure 4.16 Abrasion wear graph of SS316L specimens through MAX HD 35 particles.**

For WED 430 particles (Figure 4.17), the HT abrasion wear showed an initial increase in mass and then a decrease. The specimens gained oxides up to around 50 hours before layers were continually removed until 500 hours. Then oxides started to build up and stayed because of the strength of the oxide layers. The LT test showed mostly a decrease with one spike which could be attributed to measuring error.

All of the graphs in this section showed how much temperature effected the interaction between specimens and particles. When abrasion wear increased due to oxidation built up or decreased due to erosion, it showed that temperature plays a role on

whether there is a gain or loss in the specimens' mass. Particle shape and size played an effect on how temperature affects the specimen, verifying how results are different in same specimens but different particles.

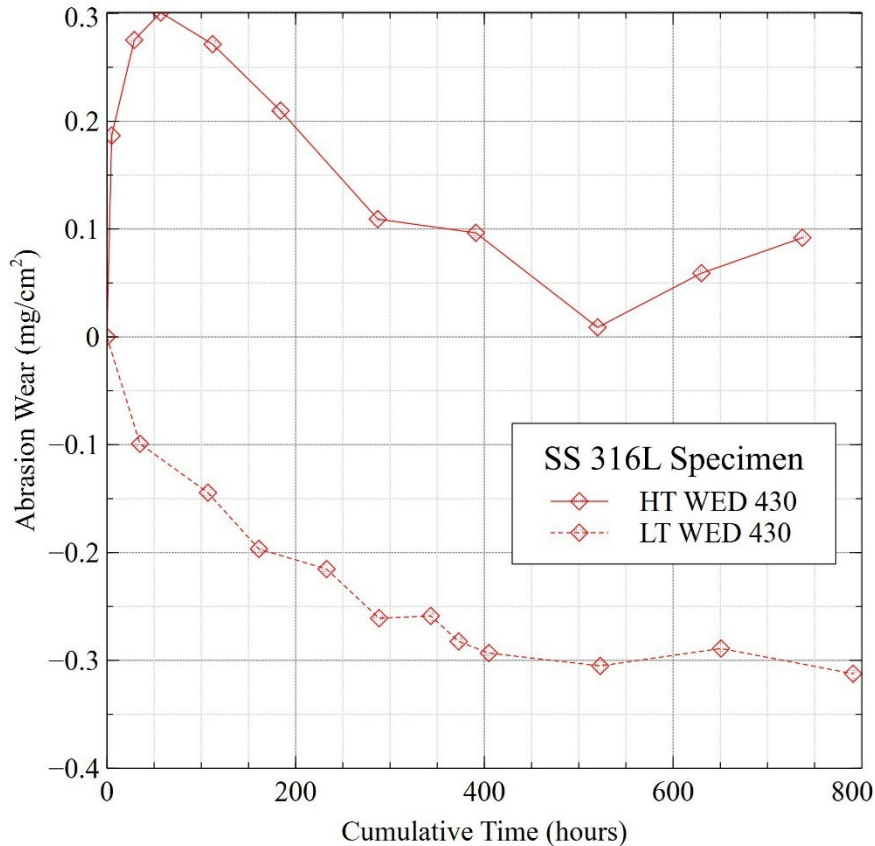


**Figure 4.17 Abrasion wear graph of SS316L specimens through WED 430 particles.**

#### **4.6 Effect of Rotation at HT**

##### Comparison of Weight Change due to Rotation

Galiullin tested austenitic and martensitic steels at different temperatures [19]. The differences between Galiullin's test and the current tests can be found in Table 4.5. The table includes speed of rotation, the rate at which the specimen was submerged, temperature of kiln, type of particles, type of materials, and how big the leading-edge surface was. The last column of the table refers to which test would go through more

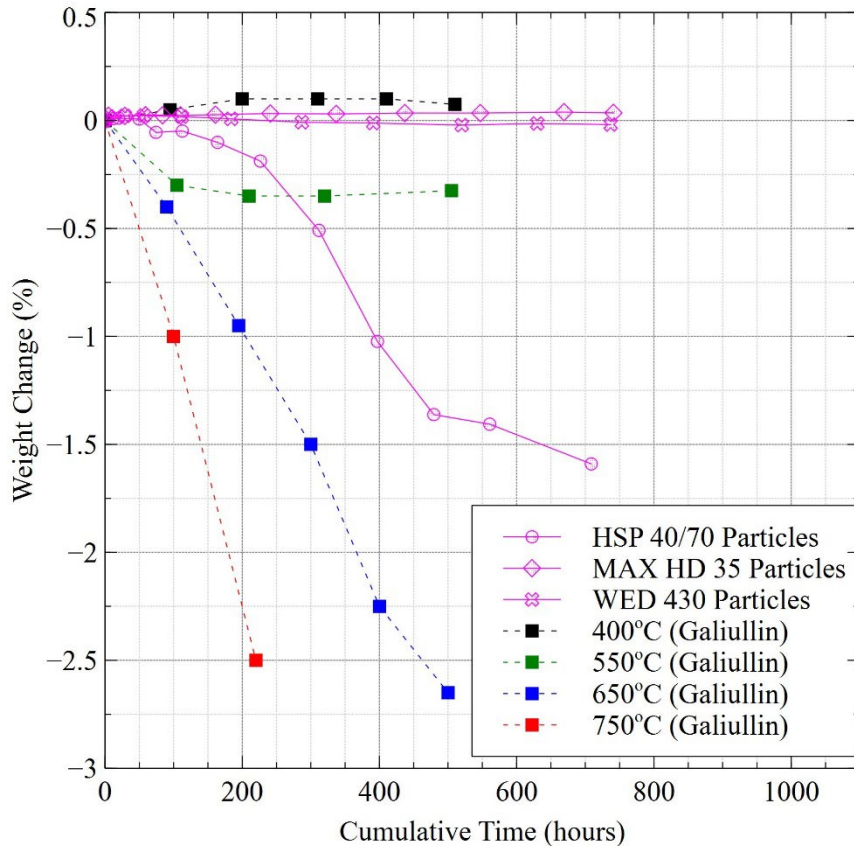
abrasion wear based on that factor. For example, the speed of rotation of Galiullin's test versus the current test is 3.0 and 1.5 cm/s respectively. Based on previous research about velocity, and how speed impacts erosion, Galiullin's test would undergo more abrasion wear. The HSP 40/70 particles used in the experiment were a type of sintered bauxite particles so it is comparable to Galiullin's particles, although Galiullin's particles are not fully specified. The results found in Figure 2.13 are martensitic steel results. SS316L is an austenitic steel with a lower carbon content and is more corrosive resistance.

**Table 4.5 Comparison of Galiullin's test to the current testing parameters.**

<b>Factor</b>	<b>Galiullin Test</b>	<b>Current Test</b>	<b>Predicted Abrasion Wear</b>
Speed of Rotation (cm/s)	3.0	1.5	Galiullin
Specimen Submerged Rate	Submerged 100%	Submerged 50%	Galiullin
Temperature (°C)	Maximum of 750	800	Current
Particles	Sintered bauxite	Multiple	Depends
Material	Martensitic steel	Austenitic steel	Galiullin
Leading Edge Surface Area (in <sup>2</sup> )	0.308	0.125	Galiullin

Based on all the factors, it seems that Galiullin's test would undergo more abrasion wear. The results calculated are based on weight change which is found by Equation 4.1, where  $m_e$  is the mass at the hour calculated and  $m_0$  is the initial mass before testing the specimen.

$$\text{weight change (\%)} = \frac{(m_e - m_0)}{m_0} * 100\% \quad (4.1)$$



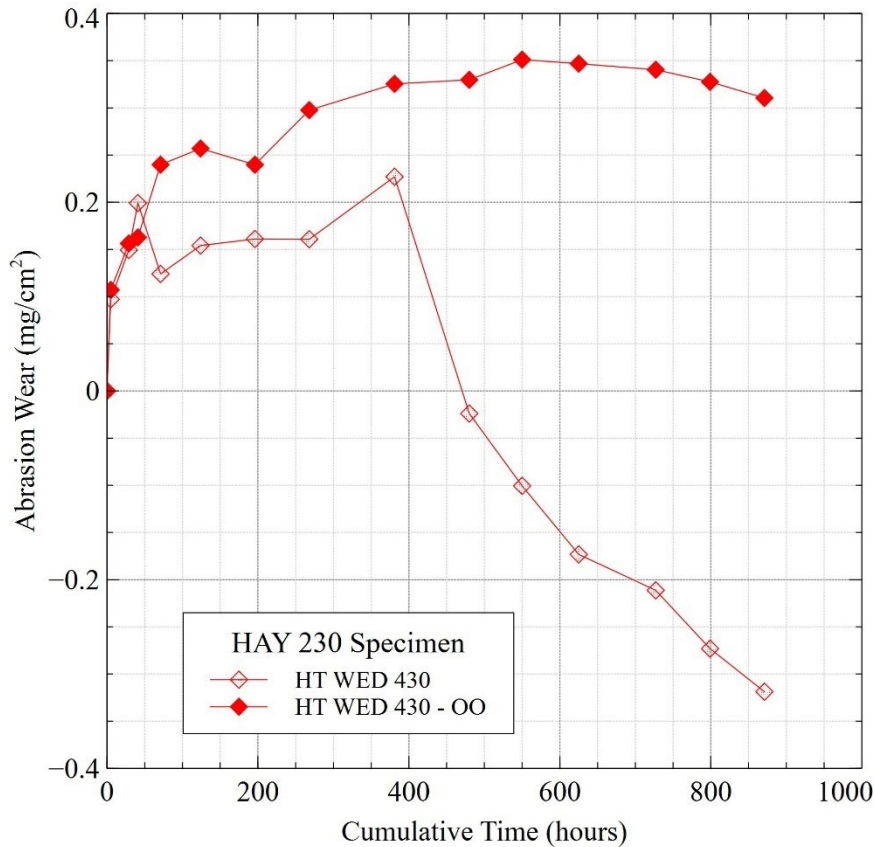
**Figure 4.18** Averaged weight change of SS316L specimens through different particles compared to an edited graph of Galiullin's work of martensitic steel from Figure 2.13.

Figure 4.18 shows the weight change of SS316 specimen experiments running through different particles at a temperature of 800°C. It was compared to Galiullin's results at different temperatures. Galiullin's results are divided in half to show what the weight change would be based on Galiullin's test being submerged only half the time instead of 100% of the time. The experiments completed during this test were mostly similar, with very little weight change, having a maximum of -1.6% weight change for HSP 40/70 particles. If the HSP 40/70 test continued, there would probably be a continued slope

downwards. These results make sense because all the different factors added together would have Galiullin's test undergo around three times more of a weight change than current tests.

### Oxidation and Rotation

Movement of the specimen through the particles created more abrasion wear compared to specimen that did not rotate. OO specimen was compared with the specimens inside the kiln that rotated. For the HAY230 specimens test running through WED 430 particles, the OO specimen had an abrasion wear of  $0.31 \text{ mg/cm}^2$  while the average rotating specimen had an abrasion wear of  $-0.32 \text{ mg/cm}^2$  (Figure 4.19). This is valid compared to the research above. The OO specimen sat in the back of the kiln and oxides built up on the specimen over time. The rotating specimens had an initial increase in oxides but over time, the oxides wore down and sheared off in one chunk. This is shown in the drop that occurs in the rotating specimens around 400 hours.



**Figure 4.19 Abrasion wear of HAY230 specimen in WED 430 particles.**

For the SS316L specimens, the test in WED 430 and HSP 40/70 #2 particles follow the same trend (Figure 4.20 and Figure 4.21) as the HAY230 graph did (Figure 4.19). There was an initial increase in mass due to a buildup of oxides but it quickly sheared off and additional oxide layers did not play a significant effect. Erosion occurred as the specimens continued to lose mass. For the OO specimen in Figure 4.20, oxides built up on the surface throughout the whole experiment.

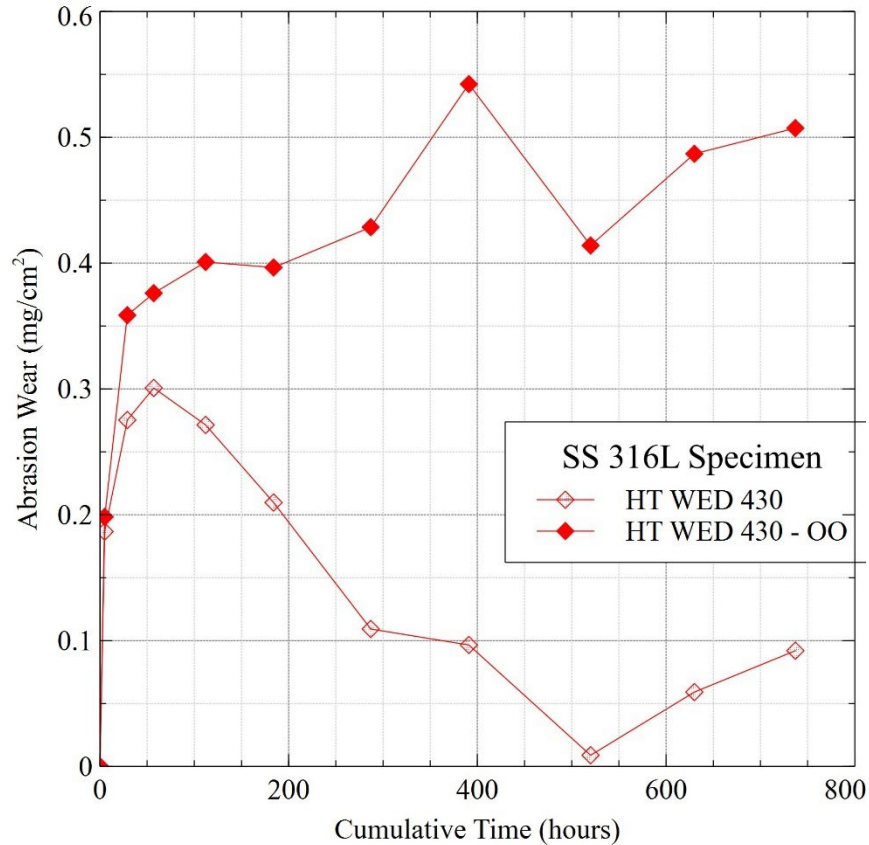


**Figure 4.20 Abrasion wear of SS316L specimen in WED 430 particles.**

The HSP 40/70 #2 particle graph (Figure 4.21) shows each SS316L specimen by itself instead of the average of the SS316L specimens. The colors and shapes are different in this graph to highlight the differences and similarities. In this case, all the specimens follow the same slight increase, followed by a decrease in abrasion wear. In the OO specimen, oxides built up but sheared off and lost mass. Since the OO specimen was not undergoing a rotation, the decline is due to the removal of spalling and oxides, likely with shop air.

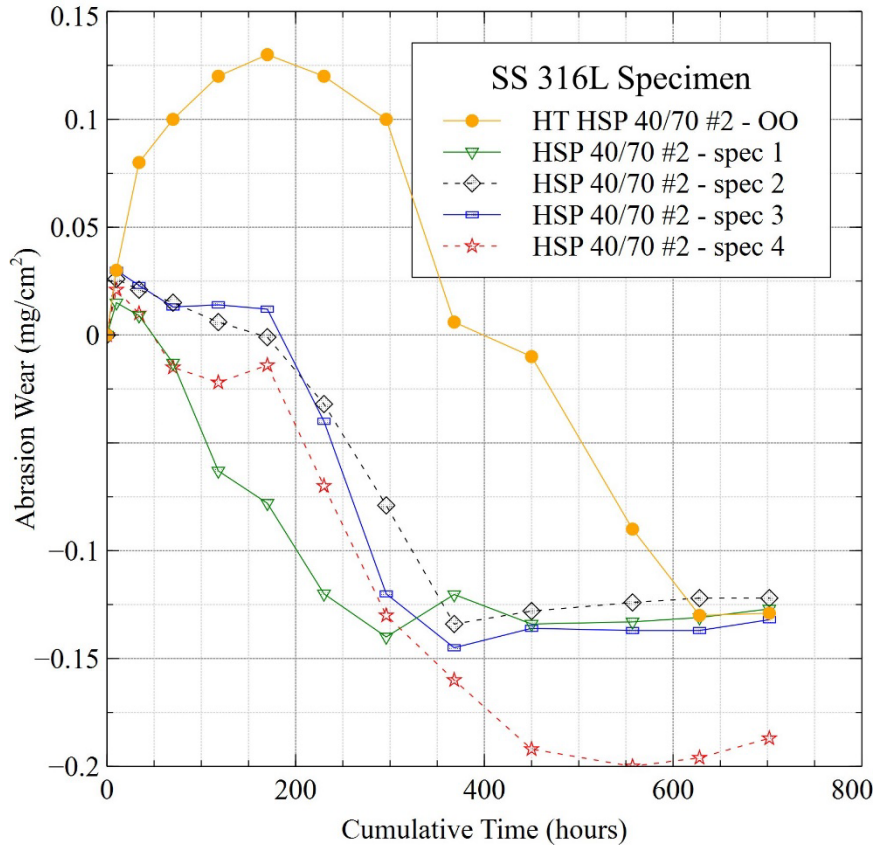


**Figure 4.21 Abrasion wear of SS316L specimen in HSP 40/70 #2 particles.**

The unique set of particles was the MAX HD 35 particles (Figure 4.22). The OO specimen gained less mass than the rotating specimen. This could be due to a bigger buildup of oxides on the rotating specimen that were never able to come off, even with the rotation it was undergoing. This could refer to Stott's thoughts on the strength of oxidation layers and how some layers can be stronger than others. The strong layers take more work to get off.

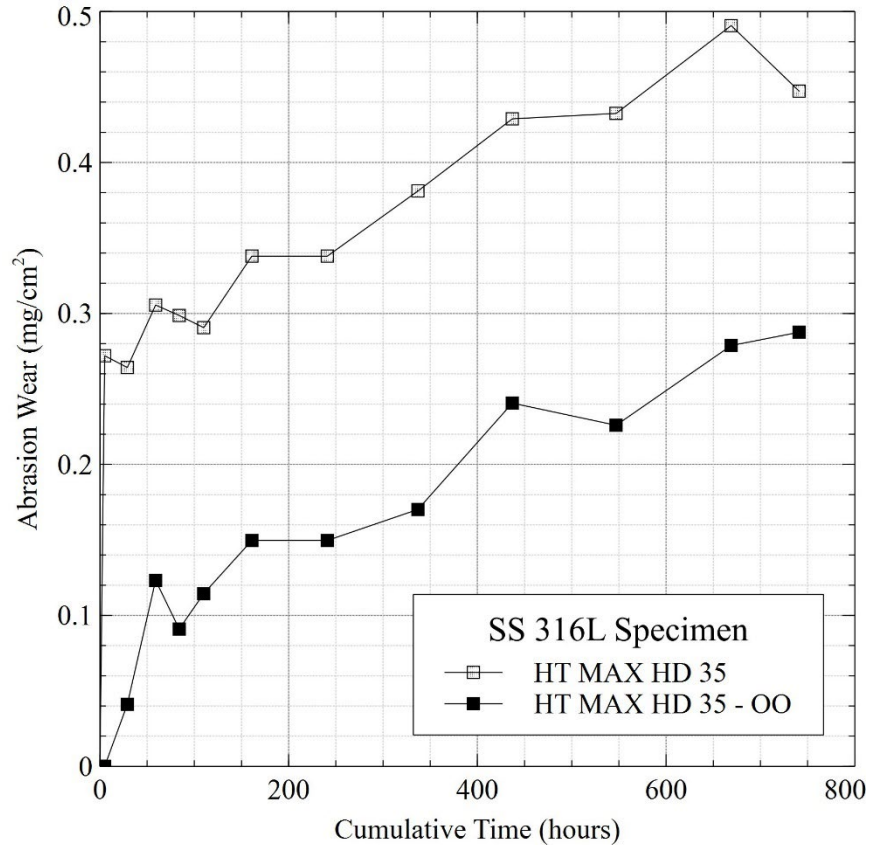


**Figure 4.22 Abrasion wear graph of SS316L running through MAX HD 35 particles.**

Rotation plays a key role, either adding layers of oxides or wearing down the material. It depends on the strength of the oxidation level and how easy it is to shear off.

Another test to determine abrasion wear based on oxidation and high temperature is to find the synergy value [18]. The synergy value is found based on the abrasive wear found in the rotating specimens and corrosion which is found in OO specimen. Table 4.6 shows the synergy values at the end of the experiments.

**Table 4.6 Synergy values of different specimens.**

<b>Specimen</b>	<b>Particle</b>	<b>Synergy Value</b>
SS316L	HSP 40/70	40.14
	MAX HD 35	1.56
	WED 430	0.181
	HSP 40/70 #2	1.231
IN740H	HSP 40/70	9.574
	MAX HD 35	0.990
SS316H	WED 430	0.601
HAY230	WED 430	1.027

If the synergy value is greater than 1, abrasion wear is affected by the particles. Some synergy values are close, for example, HAY230 is 1.027. Based on the synergy values, HSP 40/70 particles had the most effect on specimens compared to the other particles. This shows the synergy values are dependent on what particles are being used but more research is required to before coming to a complete conclusion.

#### **4.7 Abrasion Wear Question Regarding SS316L**

As stated before in the analysis with Huang, there is a big difference in weight change in HSP 40/70 particles compared to the other particles (Figure 4.18) when looking at SS316L specimens. Looking at the abrasion wear graph, SS316L specimens have a greater abrasion wear with HSP 40/70 particles (Figure 4.23).

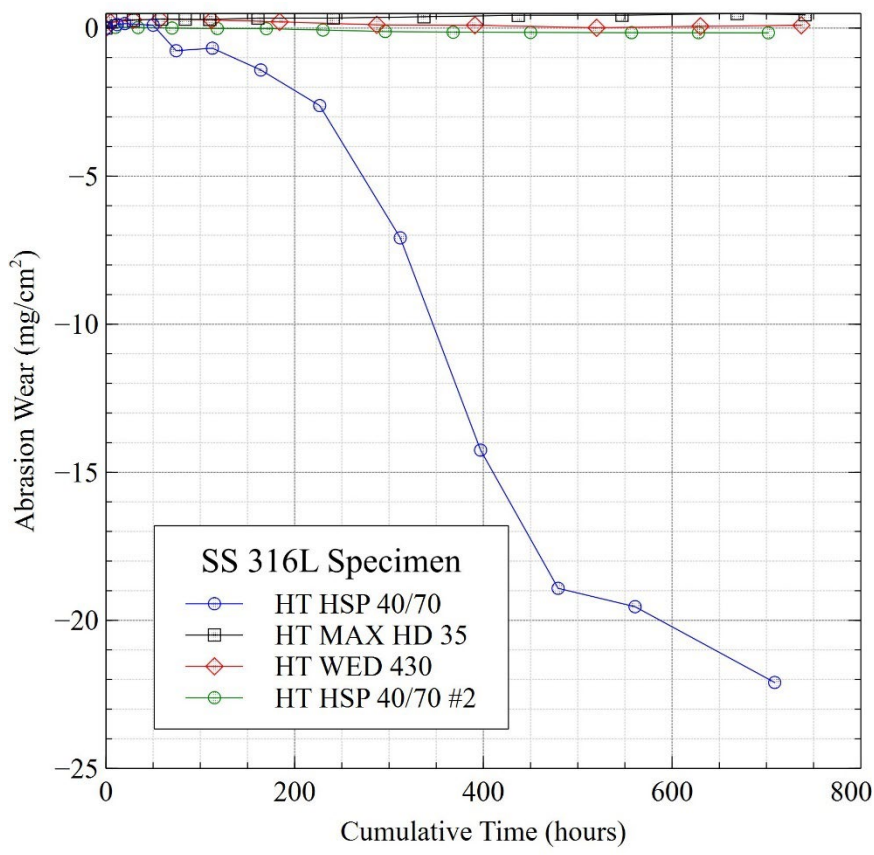


**Figure 4.23 Abrasion wear of SS316L specimen for HT only,**

In the HT HSP 40/70 particle test, there is  $-22 \text{ mg/cm}^2$  in abrasion wear while the other tests have under  $-1 \text{ mg/cm}^2$  or an increase in abrasion wear. The graph of the HT data can be shown more accurately when zoomed in (Figure 4.24). An additional test with HSP 40/70 particles (referenced HSP 40/70 #2) and SS316L specimens was completed and it still did not have the amount of abrasion wear as the first HSP 40/70 particle test.

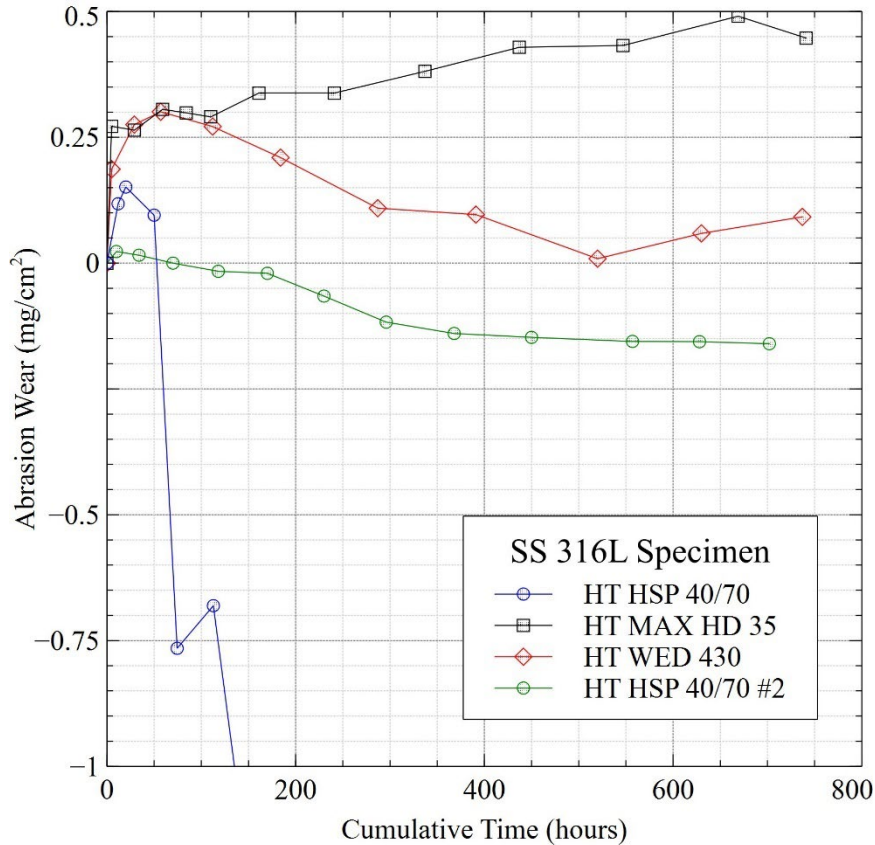


**Figure 4.24** Abrasion wear graph of Figure 4.23 zoomed in.

It is important to analyze the data from the HSP 40/70 test as it is different from the others. For HT testing, the experiments went in the following order with respect to SS316L: HSP 40/70, MAX HD 35, WED 430, and HSP 40/70 #2.

There was some speculation on what was happening and why the HSP 40/70 results underwent more abrasion wear. Hypotheses include the error, the material, cumulative cycles during a test, and oxidation build up in the apparatus.

### Error of Testing

As stated earlier, the error of most measurements of specimens have a maximum error of  $\pm 0.0006$ . This error is small enough that it does not play an effect on the results. In the HSP 40/70 test, two errors are 0.0017 and 0.0026 for 50 and 74 hours respectively. Figure 4.25 shows the SS316L specimen running through only HSP 40/70 particles. The

error occurred earlier on and did not have an effect on the major drop that started at around 250 hours. Therefore, the error in measurement did not contribute to the conclusion of the SS316L specimens.

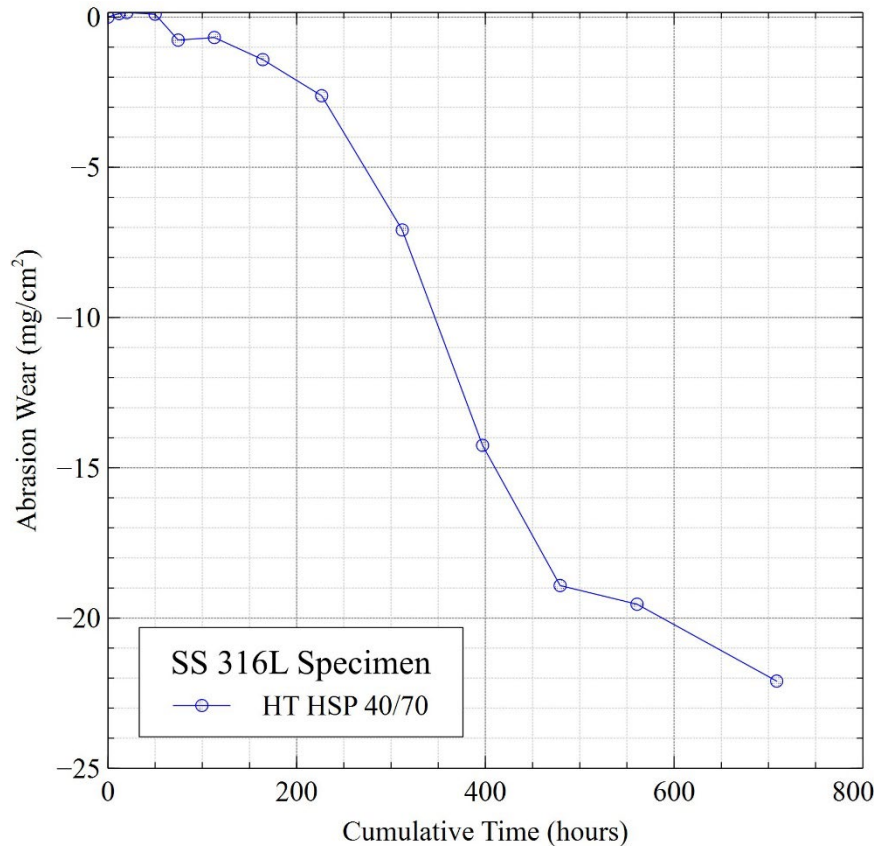


**Figure 4.25 SS316L specimen in HSP 40/70 for HT to show effect of error.**

### SS316L Material

All SS316L material was bought from McMaster-Carr as bar stock with 0.5” width and 0.25” thickness. Two different bar stocks were bought. There was no additional preparation besides using the band saw, and the alcohol after drilling and tapping. Surface finishes of the material was viewed. Looking back at all the specimens, there were two main surface finishes, a rough surface finish and a linear smooth surface finish. The rough

surface finish was rough all around (Figure 4.26a) while the smooth surface finish had a little roughness going one way but was smooth going the other way (Figure 4.2b).



(a)



(b)

**Figure 4.26 SS316L (a) rough and (b) smooth surface finishes.**

Once all the material was rechecked, it was found that most surfaces had one rough and one smooth surface finish but there were a few specimens that had either two rough or two smooth surface finishes. There is no way of knowing which material came from which bar stock because it got mixed together without the initial check.

#### Cumulative Cycles

Another possible reason is the number of cumulative cycles. As stated before, a cycle is defined as the kiln starting at  $\sim 20^{\circ}\text{C}$ . The kiln is turned on with the apparatus, specimens, and particles inside and is heated to  $800^{\circ}\text{C}$  in the span of two hours. Once the kiln reaches  $800^{\circ}\text{C}$ , the motor turns on and the specimens begin to rotate in the apparatus. The specimen rotate for however long the kiln is turned on for. Once the time allotted is complete, the motor turns off, the specimens stop rotating, and the kiln turns off. It then takes the kiln 8-10 hours to cool back down to  $\sim 20^{\circ}\text{C}$ .

The HSP 40/70 particle test was the first test ran in the kiln. The test did not immediately run in 24-hour increments. Due to preliminary testing and restrictions on run

time, the kiln only ran a maximum of 8 hours a day. This means that the first test went through many more cycles than the other tests.

The graph shows a comparison between cumulative cycles in an experiment and abrasion wear (Figure 4.27). The first test had many more thermal cycles and also had the massive abrasion wear.

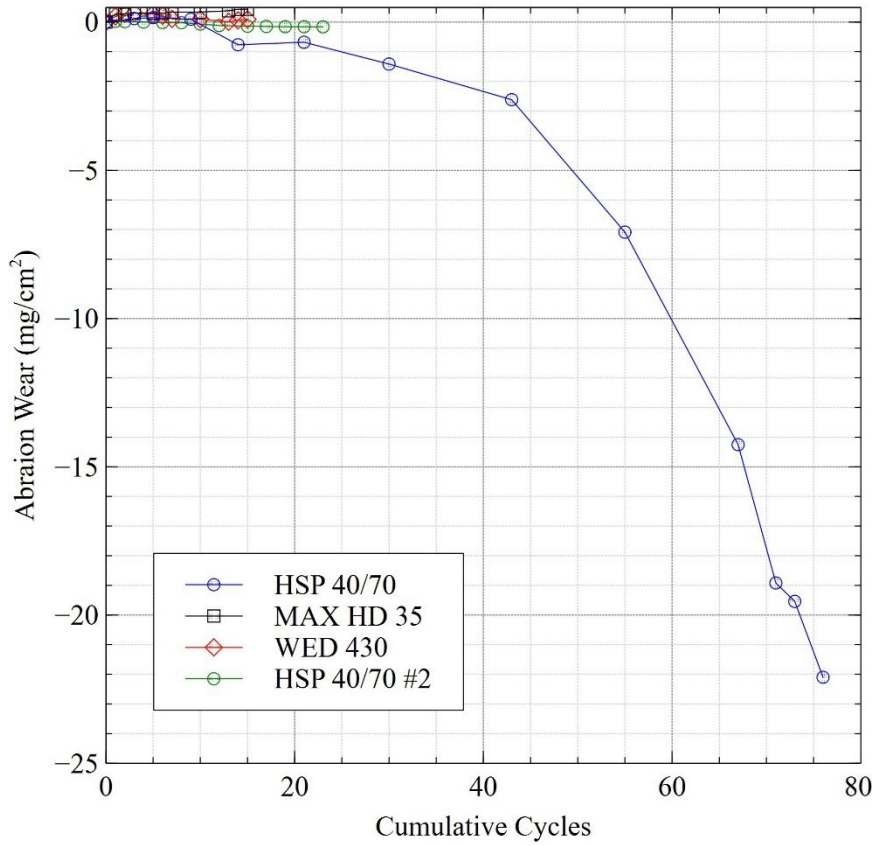


**Figure 4.27 Abrasion wear vs cumulative cycles for SS316L specimen tests.**

This seems improbable, as for the HSP 40/70 #2 particle test, the abrasion wear does not begin to rapidly decrease like the HSP 40/70 particle test did, even though both tests were ran the same number of cumulative hours.

### Increase of Oxides

The last and most probable reason for the abrasion wear difference is due to oxidation build up. Initially the apparatus ran without an experiment. It ran a few thermal cycles to make sure it was working and to burn off any small particles that may have built up during the building and welding of the apparatus. The trough that the particles lay in is made of SS316L material. Most likely, the apparatus did not go through enough thermal cycles and oxides from the inner part of the trough came off. The oxides mixed in with the particles as the specimens rotated in and out of the trough.

With all the additional oxides, there was not only specimen to particle interaction, but also specimen to SS316L oxide interaction. Figure 4.1 showed untested HSP 40/70 particles. Figure 4.28 shows HSP 40/70 particles after the first abrasion test was complete with SS316L specimens. Figure 4.29 shows HSP 40/70 #2 particles from the second abrasion test with SS316L specimens.



**Figure 4.28** Image of HSP 40/70 particles.



**Figure 4.29** Image of HSP 40/70 #2 particles.

As shown, Figure 4.28 has an increase in oxides, both in the number of oxides and the size of the oxides compared to Figure 4.29. This could have a significant impact if that number of oxides was scattered throughout all the particles and SS316L specimens were rotating in and out of it.

#### **4.8 Surface Profilometry on SS316L**

Surface profilometry was completed on the finished SS316L specimens. Each test had a specimen drawn at random to be used. The instructions from Chapter 3.6 were followed. The distance found in each spot (the middle and the edge) was based on the lowest valley and the highest peak in the image and the average roughness was found over the total surface (Table 4.7).

**Table 4.7 Analysis of Surface Profilometry for SS316L**

<b>Particles Ran Through</b>	<b>Middle Distance (<math>\mu\text{m}</math>)</b>	<b>Middle Surface Avg Roughness (<math>\mu\text{m}</math>)</b>	<b>Edge Distance (<math>\mu\text{m}</math>)</b>	<b>Edge Surface Avg Roughness (<math>\mu\text{m}</math>)</b>
Untested	19.5	2.29	18.6	1.88
MAX HD 35	16.1	1.70	15.2	1.43
WED 430	13.6	0.963	18.1	2.26
HSP 40/70	16.4	1.59	16.4	1.70

In all cases, the untested specimen had more of a distance between the highest peak and lowest valley in both the middle and the edge images. For all the tests except WED 430 particles, the tested specimen average roughness was less than the untested specimen. Despite the high repeatability, this data is not fully reliable. Unfortunately, this data cannot prove if there is wear on the specimen. Since there is no chemical analysis, either the specimens could have gone through wear or the specimens could have gotten a layer of oxide that also smoothed out the surface. In previous research, it was found that even though the specimens were from the same company, there were rough and smooth surfaces on different specimens that supposedly came from the same bar stock. This was not considered when conducting surface profilometry. Additional images of the surfaces can be found in Appendix B.

#### **4.9 Cross-Sectional SEM Imaging**

SS316L and IN740H specimens were analyzed at from the first HSP 40/70 particle test (Figure 4.30 and Figure 4.31). HAY230 specimen from the WED 430 particle test was also analyzed (Figure 4.32). The blue arrow shows the surface of the material. The material

on each surface is not completely straight. This shows that the material did wear down over time. There is also a purple arrow that describes the layer of oxides. The thickness of the oxide layer is dependent on the type of material used. This confirms what Stott said and shows that oxidation is occurring continuously throughout the tests, especially since there was still oxide present at the end of the experiment. The SS316L specimen image (Figure 4.30) has a yellow arrow. That refers to an additional layer of oxides built up on top of the previous layer of oxides, which also follows Stott's conclusions.

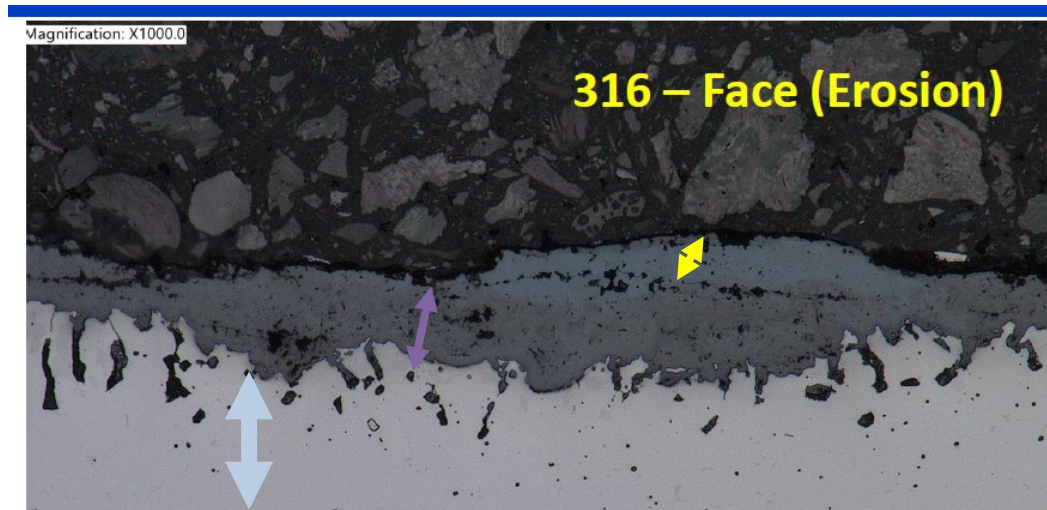


**Figure 4.30** Cross-sectional SEM of SS316L in HSP 40/70 particles.

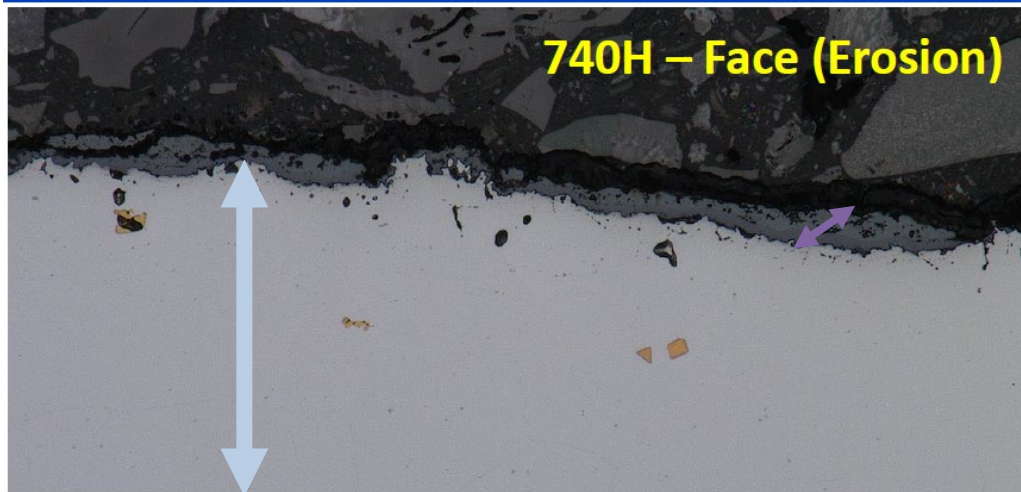


**Figure 4.31** Cross-sectional SEM of IN740H in HSP 40/70 particles.

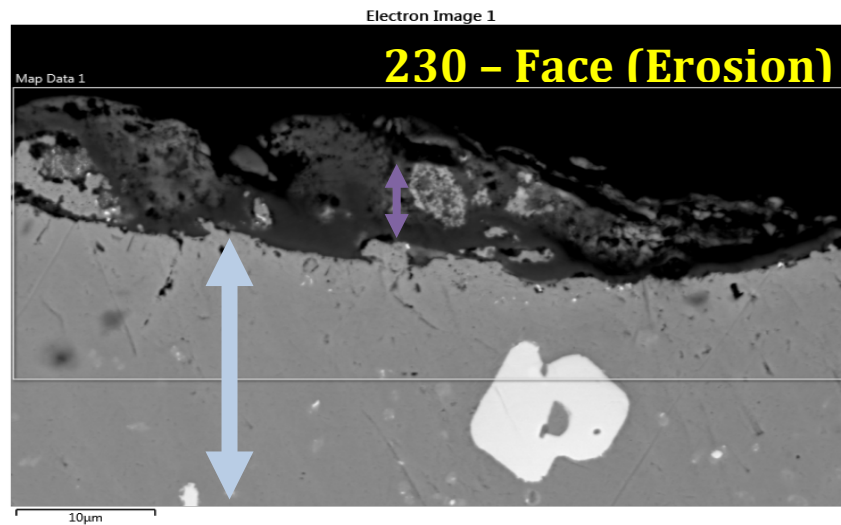


**Figure 4.32** Cross-sectional SEM of HAY230 in WED 430 particles.

### Chemical Composition

Chemical composition looks at the chemical make-up of an cross-sectional SEM image (Figure 4.33). For example, Figure 4.32 shows a HAY230 specimen that has been through WED 430 particles. The image can be analyzed via the chemicals each section is composed of.

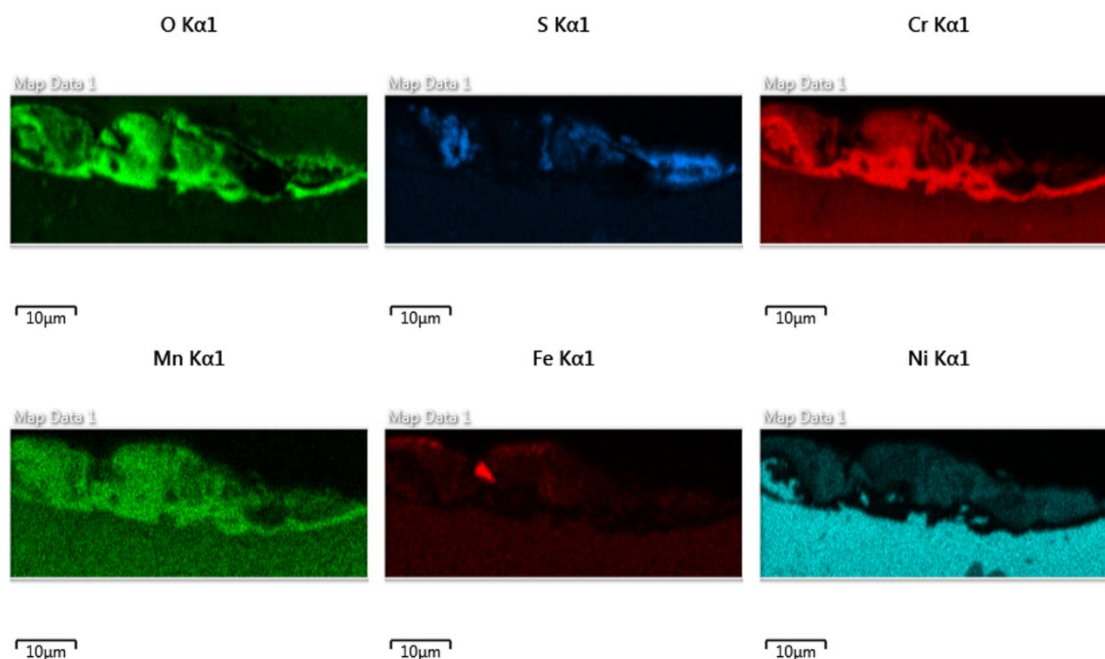


**Figure 4.33 Chemical composition of cross-sectional SEM of HAY230.**

The chemical composition shows that oxidation layer was mainly made of oxygen. This helped confirm that the oxidation layer is actually made of oxides due to the high levels of oxygen in the kiln. The oxide layer also had lots of chromium. The composition shows that the base layer of HAY230 specimen was made up of a lot of nickel. This is positive and proves the surface is HAY230 because HAY230 is mostly made of nickel.

#### 4.10 Reflectance

Reflectance is taken on the particles after they finish their experiment. Reflectance of HSP 40/70 particles are found in Figure 4.34.

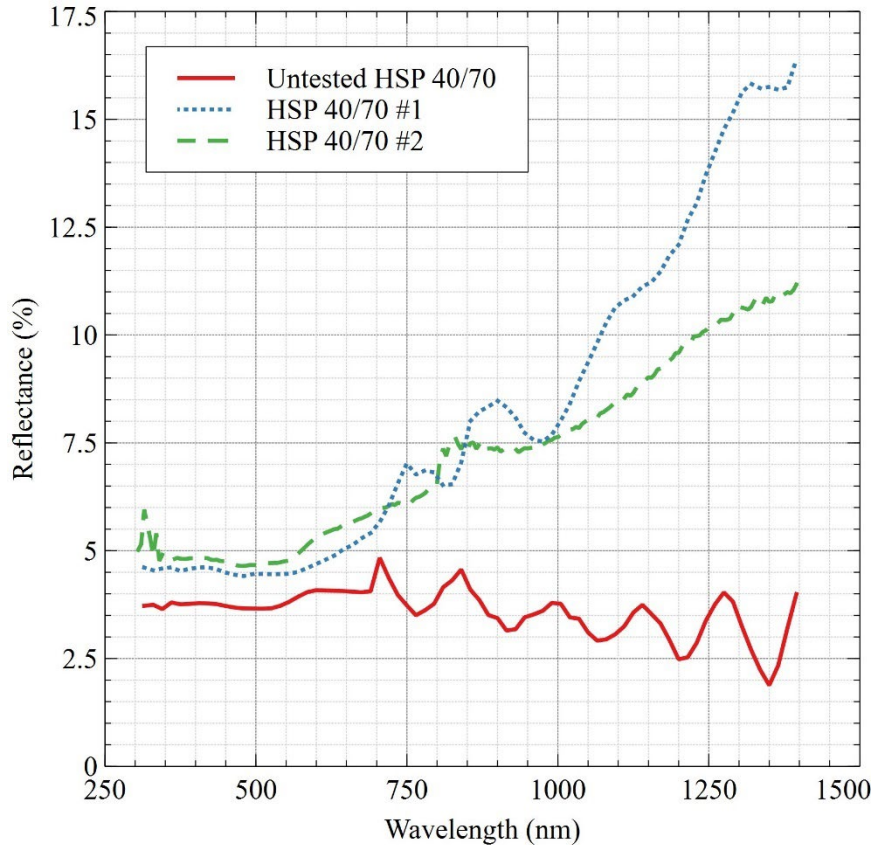


**Figure 4.34 Reflectance of HSP 40/70 particles between two different HT tests.**

The first HSP 40/70 test has a much higher reflectance in the infrared than the HSP 40/70 #2 test and the untested particles. This could be from the extra oxides that were found in the first test but more oxides need to be collected and reflectance done on them to prove this.

#### 4.11 Particle Size Analysis

Particle size analysis was done on the abrasion particles. A sample of the HSP 40/70 particle tests were taken. The image initially looked like Figure 4.35.

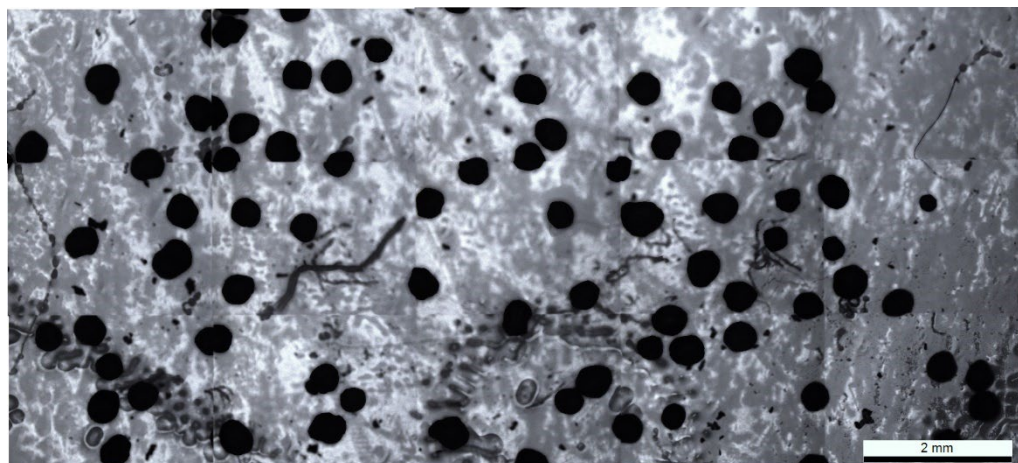


**Figure 4.35** Leica microscope image of HSP 40/70 untested particles.

The particles got inserted into ImageJ and Figure 4.36 was found by taking a sample of the particles. It was made sure that no oxides were considered in the analysis and only whole particles were considered. (If any part of the particle was cut off due to the image or the Power Mosaic feature, it was not included.)

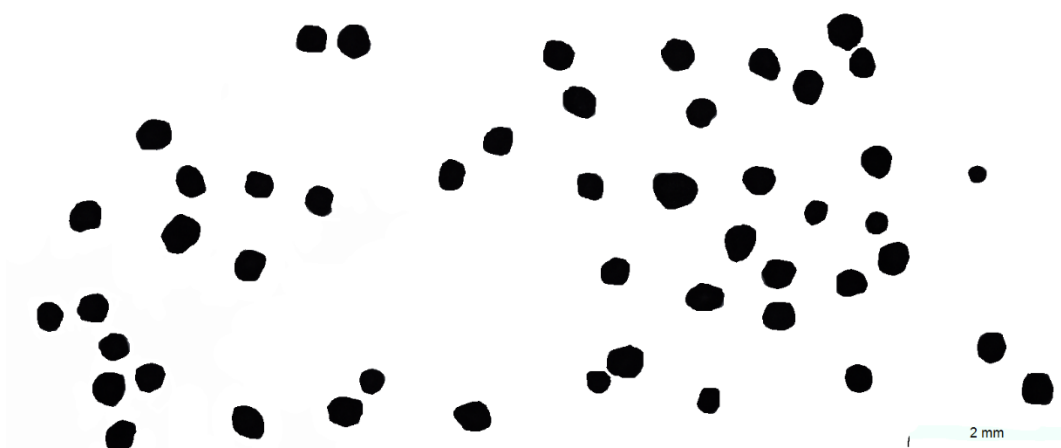


**Figure 4.36** Image of same particles in Figure 4.35 after omitting particles.

Then, the particles were put through the analysis and circularity, Feret diameter, etc. were calculated. Each particle was accounted for, as shown in Figure 4.37.

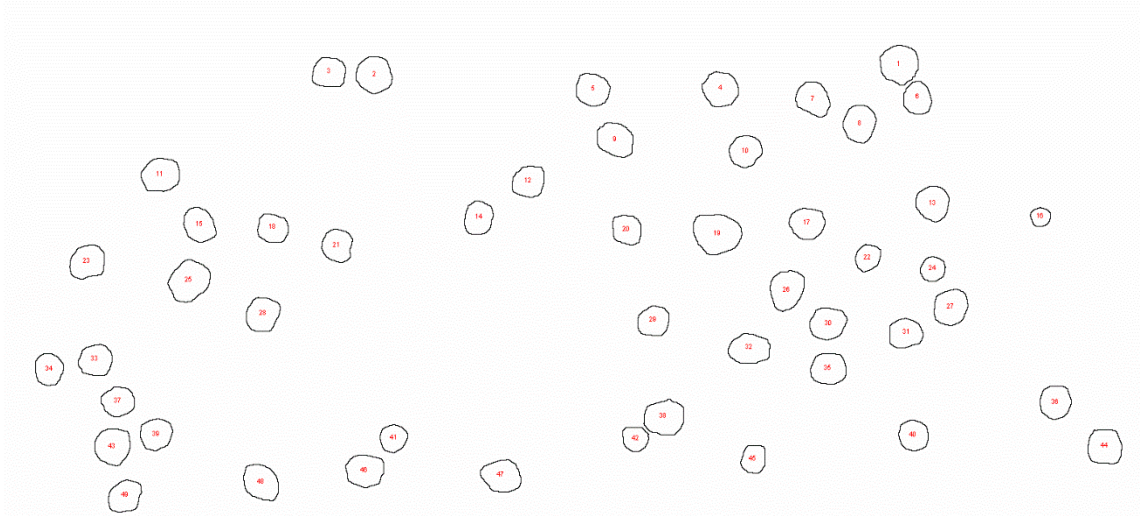


**Figure 4.37** Outline of Figure 4.36 of the particles labeled that were considered.

This process of particle analysis happened for all the particles and the results can be found in Table 4.8.

**Table 4.8** Analysis of HSP 40/70 particles.

Test	Untested	HSP 40/70 #1	HSP 40/70 #2
Sample Size	49	64	59
Average Area (mm <sup>2</sup> )	0.1190	0.1000	0.0985
Standard Deviation of Area (mm <sup>2</sup> )	0.0287	0.0260	0.0306
Feret Diameter (mm)	0.4355	0.4017	0.3931
Standard Deviation of Feret Diameter (mm)	0.0594	0.0546	0.0627
Circularity	0.8775	0.8772	0.8840

These results show that there is not much change in particles. The circularity stayed pretty consistent among all the different tests. The HSP 40/70 #2 particle test had a smaller average area and a smaller ferret diameter compared to the others but it also had larger

standard deviations, meaning the particles were not as precise. From untested to testing of 700+ hours, there was very little change. The particles did not undergo a lot of wear.

#### **4.12 Summary**

There was a lot to uncover in the results and analysis of the data. There was data and it proved the works of Huang in regards to oxidation analysis, Lin in regards to the effects of particle shape and size, Stott in regards to the work on oxidation layers, and Galiullin in regards to the conducted CSP experiment. Having different types of analysis on the particles, particle size analysis and reflectance, and specimens, surface profilometry and cross-sectional SEM, were beneficial because they all played a part into understanding the abrasion wear and material degradation at HT.

## CHAPTER FIVE: CONCLUSION

### 5.1 Work Completed

The following main conclusions were drawn from the results, analysis, and work completed regarding abrasion and the wear between material and particle interaction and degradation.

- Running tests at 800°C had a significant effect, whether it was due to oxidation or erosion on the specimens. This was found in IN740H specimens at HT. When running through HSP 40/70 particles, specimens had an abrasion wear of -1.236 mg/cm<sup>2</sup>, showing erosion. When running through MAX HD 35 particles, specimens had an abrasion wear of 0.1927 mg/cm<sup>2</sup>, showing oxidation.
- Oxidation is built up in specimens. For SS316L specimens running through MAX HD 35 particles, the abrasion wear was 0.4473 mg/cm<sup>2</sup> for HT, -0.1360 mg/cm<sup>2</sup> for LT, and 0.2876 mg/cm<sup>2</sup> for OO specimen. This followed along with Huang's tests that ran for 1000 hours where the weight change was 0.05 mg/cm<sup>2</sup> for the 400°C experiment and 1.35 mg/cm<sup>2</sup> for the 800°C experiment. Oxides became strong and held onto the HT and OO specimens, like proven by Stott.
- The particles itself are sturdy and has a small erosion ratio at HT. This was shown in the circularity of HSP 40/70 untested, test 1 (709 hours), and test 2 (702 hours) images respectively, 0.8775, 0.8772, and 0.8840.

Abrasion erosion mostly had very small abrasion wear rates. This showed that when looking at the types of erosion (impact, abrasion, and attrition), abrasion erosion does not

make a huge difference in material and particle degradation. The other types of erosion need to be analyzed to see if solid particles are a good HTM.

The work completed has helped the CSP community and future research. Sandia National Laboratories has been awarded funding to continue their research by building a CSP infrastructure using solid particles as the HTM. Them, along with other researchers can use this information to pick out materials, along with comparison for future research on how material degradation is affected by high temperatures.

## **5.2 Limitations**

Despite all that has been done, there has been many limitations on the work completed. One big limitation was consistency throughout all the tests. Each test was running about the same number of hours but the variation on how often each test was ran could affect it. For example, measurements for HT were made every three to 100 hours of run time whereas LT measurements mostly occurred every 24 hours. The number of cycles could have impacted the work. For example, the first test was run over a total of 80 thermal cycles while others were only run around 20. In addition, not all specimens were from the same place. Buying stock from a certain vendor narrows the differences but there could be differences on surface finishes that could have affected the results. Other research tests, such as Wilson, has sanded down their materials before testing which could potentially give specimens that are more consistent [14].

When calculating abrasion wear (Equation 3.2), the surface area of all six sides of the specimen were taken. This did not consider the differences between the leading edge and trailing edge. The leading edge would have more abrasion wear than the trailing edge and the differences were not looked at.

### 5.3 Future Work

With all the results so far, a model can be built to predict the abrasion wear of a specimen based on the mechanical properties of that material and particles being used. This model will allow all different combinations to be predicted, without going through months of testing.

More testing can be done to get accurate results. Currently a test is being ran at HT with 8 specimens of SS316L to try and determine if the smooth and rough surface finishes had an effect on the abrasion wear of the specimen. This is done by changing the orientation of specimen so that the leading edge is different. Future testing will continue through private contracting. A private company already has work set up to run additional specimen in very specific ways. The specimens are the same material with the same surface finish. Adding this data to the model can help improve the rate of prediction. With their specifications, this testing should be able to replicate easier.

Additional testing can also bring more results regarding oxidation. Oxidation was found to form on the specimen and stay on the specimen, even at the end of the experiment. Testing more consistently, along with surface profilometry and cross-sectional SEM throughout the experiments could help identify exactly how the oxides grow and leave the specimen over time.

Additional analysis can also be done on the data already received. The specimens were looked at based on the particles it went through but the particles did not play an effect on the graphs.

Future work should test the specimens for longer. Most tests ran an average between 500-800 hours of run time. In a few of the specimens, the graphs reached a steady

state. If more hours were run, it could be verified if another steady state was reached or if once the specimen reaches steady state, it stayed steady state the whole time. The understanding of oxides and how they build could affect the potential steady state results.

## REFERENCES

- [1] N. Kh. M. A. Alrikabi, “Renewable Energy Types,” *Journal of Clean Energy Technologies*, pp. 61–64, 2014, doi: 10.7763/jocet.2014.v2.92.
- [2] Solar Energy Technologies Office, “Solar Energy in the United States,” 2022.
- [3] D. Barlev, R. Vidu, and P. Stroeve, “Innovation in concentrated solar power,” *Solar Energy Materials and Solar Cells*, vol. 95, no. 10. Elsevier B.V., pp. 2703–2725, 2011. doi: 10.1016/j.solmat.2011.05.020.
- [4] Z. Ma, G. Glatzmaier, and M. Mehos, “Fluidized bed technology for concentrating solar power with thermal energy storage,” *Journal of Solar Energy Engineering, Transactions of the ASME*, vol. 136, no. 3, 2014, doi: 10.1115/1.4027262.
- [5] A. Calderón, C. Barreneche, A. Palacios, M. Segarra, C. Prieto, and A. Inés Fernández, “Review of solid particle materials for heat transfer fluid and thermal energy storage in solar thermal power plants.,” 2019. [Online]. Available: <https://mc.manuscriptcentral.com/LongRequest/est2?DOWNLOAD...>
- [6] A. Calderón *et al.*, “High temperature systems using solid particles as TES and HTF material: A review,” *Applied Energy*, vol. 213. Elsevier Ltd, pp. 100–111, Mar. 01, 2018. doi: 10.1016/j.apenergy.2017.12.107.
- [7] C. Ho *et al.*, “Technology advancements for next generation falling particle receivers,” in *Energy Procedia*, Jan. 2014, vol. 49, pp. 398–407. doi: 10.1016/j.egypro.2014.03.043.
- [8] M. Mehos *et al.*, “Concentrating Solar Power Gen3 Demonstration Roadmap,” Golden, CO (United States), Jan. 2017. doi: 10.2172/1338899.
- [9] I. Finnie, “Erosion of Surfaces By Solid Particles,” *Wear*, pp. 87–103, 1960.

- [10] A. Yabuki, K. Matsuwaki, and M. Matsumura, "Critical impact velocity in the solid particles impact erosion of metallic materials." [Online]. Available: [www.elsevier.com/locate/wear](http://www.elsevier.com/locate/wear)
- [11] N. Lin, H. Arabnejad, S. A. Shirazi, B. S. McLaury, and H. Lan, "Experimental study of particle size, shape and particle flow rate on Erosion of stainless steel," *Powder Technology*, vol. 336, pp. 70–79, Aug. 2018, doi: 10.1016/j.powtec.2018.05.039.
- [12] H. Arabnejad, S. A. Shirazi, B. S. McLaury, H. J. Subramani, and L. D. Rhyne, "The effect of erodent particle hardness on the erosion of stainless steel," *Wear*, vol. 332–333, pp. 1098–1103, May 2015, doi: 10.1016/j.wear.2015.01.017.
- [13] M. Divakar, V. K. Agarwal, and S. N. Singh, "Effect of the material surface hardness on the erosion of AISI316," in *Wear*, Jul. 2005, vol. 259, no. 1–6, pp. 110–117. doi: 10.1016/j.wear.2005.02.004.
- [14] R. D. Wilson and J. A. Hawk, "Impeller wear impact-abrasive wear test," 1999.
- [15] F. H. Stott, "The role of oxidation in the wear of alloys," 1998.
- [16] F. H. Stott, "High-temperature sliding wear of metals," 2002. [Online]. Available: [www.elsevier.com/locate/triboint](http://www.elsevier.com/locate/triboint)
- [17] X. Huang *et al.*, "Oxidation behavior of 316L austenitic stainless steel in high temperature air with long-term exposure," *Materials Research Express*, vol. 7, no. 6, p. 66517, Jun. 2020, doi: 10.1088/2053-1591/ab96fa.
- [18] M. Antonov and I. Hussainova, "Experimental setup for testing and mapping of high temperature abrasion and oxidation synergy," *Wear*, vol. 267, no. 11, pp. 1798–1803, Oct. 2009, doi: 10.1016/j.wear.2009.01.008.
- [19] T. Galiullin *et al.*, "High temperature oxidation and erosion of candidate materials for particle receivers of concentrated solar power tower systems," *Solar Energy*, vol. 188, pp. 883–889, Aug. 2019, doi: 10.1016/j.solener.2019.06.057.

- [20] N. Goel *et al.*, “Effect of temperature on abrasion erosion in particle based concentrating solar powerplants,” *Solar Energy*, vol. 224, pp. 1127–1135, Aug. 2021, doi: 10.1016/j.solener.2021.06.080.
- [21] Solar Energy Technologies, “The SunShot Initiative,” 2022.

## APPENDIX A

Appendix A includes the all the mass of specimens from all the LT and HT experiments. Each is labeled based on the experiment the particles and specimen underwent.

**Table A.1 Specimen mass of test with HSP 40/70 particles and SS316L and IN740H specimens at HT.**

Test Time (hours)	Abrasion Wear (mg/cm <sup>2</sup> ) ± Error							
	SS316L #1	SS316L #2	IN740H #1	IN740H #2	SS316L OO	IN740H OO		
0	15.0044±0.0006	15.6734±0.0006	18.7308±0.0006	21.6734±0.0004	56.6886±0.0004	20.8390±0.0003		
12	15.0058±0.0003	15.6746±0.0002	18.7289±0.0002	21.6700±0.0002	55.7697±0.0002	20.8436±0.0002		
20	15.0061±0.0002	15.6750±0.0002	18.7291±0.0002	21.6702±0.0003	55.7694±0.0001	20.8426±0.0003		
50	15.0055±0.0017	15.6744±0.0017	18.7289±0.0017	21.6687±0.0017	55.7705±0.0000	20.8410±0.0017		
74	14.9964±0.0026	15.6645±0.0026	18.7193±0.0026	21.6587±0.0026	55.7716±0.0000	20.8318±0.0026		
113	14.9970±0.0004	15.6658±0.0003	18.7283±0.0003	21.6681±0.0004	55.7712±0.0002	20.8426±0.0004		
164	14.9914±0.0005	15.6552±0.0005	18.7272±0.0003	21.6673±0.0005	55.7695±0.0004	20.8443±0.0004		
227	14.9761±0.0003	15.6440±0.0004	18.7256±0.0004	21.6670±0.0003	59.0783±0.0002	20.8418±0.0004		
312	14.9295±0.0002	15.5921±0.0001	18.7247±0.0001	21.6642±0.0003	54.8881±0.0003	20.8414±0.0003		
397	14.8549±0.0002	15.5088±0.0002	18.7223±0.0003	21.6613±0.0001	55.7692±0.0002	20.8427±0.0002		

479	14.7803±0.0002	15.4805±0.0003	18.7222±0.0002	21.6592±0.0002	54.8857±0.0001	20.8427±0.0003
561	14.7733±0.0003	15.4739±0.0003	18.7212±0.0003	21.6583±0.0003	54.8851±0.0003	20.8429±0.0004
709	14.7451±0.0003	15.4457±0.0003	18.7186±0.0003	21.6556±0.0002	54.3673±0.0002	20.8420±0.0004

**Table A.2 Specimen mass of test with HSP 40/70 particles and SS316L and IN740H specimens at LT.**

Test Time (hours)	Abrasion Wear (mg/cm <sup>2</sup> ) ± Error					
	SS316L #1	SS316L #2	IN740H #1	IN740H #2		
0	15.6520±0.0007	15.6431±0.0008	20.5629±0.0007	20.3573±0.0008		
23	15.6527±0.0004	15.6429±0.0008	20.5662±0.0004	20.3592±0.0014		
46	15.6522±0.0003	15.6436±0.0004	20.5631±0.0005	20.3567±0.0009		
70	15.6507±0.0045	15.6377±0.0037	20.5627±0.0040	20.3595±0.0043		
92	15.6518±0.0007	15.6428±0.0007	20.5611±0.0007	20.3562±0.0006		
164	15.6497±0.0005	15.6422±0.0005	20.5618±0.0004	20.3553±0.0004		
235	15.6499±0.0005	15.6417±0.0005	20.5615±0.0005	20.3553±0.0005		

306	15.6492±0.0004	15.6416±0.0004	20.5609±0.0002	20.3553±0.0003
378	15.6493±0.0006	15.6421±0.0006	20.5604±0.0006	20.3547±0.0006
446	15.6492±0.0005	15.6418±0.0004	20.5611±0.0006	20.3548±0.0004
545	15.6483±0.0006	15.6409±0.0007	20.5589±0.0004	20.3539±0.0002
713	15.6489±0.0005	15.6415±0.0004	20.5602±0.0002	20.3545±0.0003

**Table A.3 Specimen mass of test with MAX HD 35 particles and SS316L and IN740H specimens at HT.**

Test Time (hours)	Abrasion Wear (mg/cm <sup>2</sup> ) ± Error					
	SS316L #1	SS316L #2	IN740H #1	IN740H #2	SS316L OO	IN740H OO
0	15.9168±0.0002	16.1661±0.0002	23.2222±0.0002	21.5270±0.0002	16.0700±0.0002	20.5092±0.0002
5	15.9222±0.0002	16.1677±0.0001	23.2232±0.0001	21.5268±0.0001	16.0712±0.0001	20.5080±0.0001
29	15.9221±0.0004	16.1676±0.0003	23.2223±0.0004	21.5263±0.0005	16.0717±0.0003	20.5079±0.0005
59	15.9226±0.0002	16.1681±0.0002	23.2228±0.0001	21.5270±0.0001	16.0726±0.0001	20.5086±0.0002

84	15.9226±0.0003	16.1680±0.0002	23.2227±0.0004	21.5271±0.0001	16.0722±0.0001	20.5083±0.0002
110	15.9223±0.0002	16.1681±0.0002	23.2232±0.0002	21.5273±0.0003	16.0725±0.0001	20.5089±0.0003
161	15.9227±0.0001	16.1688±0.0003	23.2235±0.0001	21.5275±0.0000	16.0729±0.0002	20.5089±0.0003
241	15.9238±0.0004	16.1695±0.0002	23.2244±0.0003	21.5284±0.0002	16.0731±0.0003	20.5092±0.0002
337	15.9236±0.0001	16.1690±0.0002	23.2241±0.0001	21.5282±0.0002	16.0731±0.0001	20.5090±0.0003
437	15.9243±0.0004	16.1696±0.0003	23.2249±0.0003	21.5292±0.0003	16.0739±0.0003	20.5102±0.0003
547	15.9241±0.0002	16.1698±0.0002	23.2256±0.0005	21.5289±0.0002	16.0738±0.0002	20.5094±0.0003
669	15.9242±0.0001	16.1711±0.0001	23.2242±0.0001	21.5296±0.0002	16.0744±0.0002	20.5101±0.0001
741	15.9240±0.0002	16.1702±0.0005	23.2248±0.0003	21.5296±0.0004	16.0745±0.0005	20.5105±0.0003

**Table A.4 Specimen mass of test with MAX HD 35 particles and SS316L and IN740H specimens at LT.**

Test Time (hours)	Abrasion Wear (mg/cm <sup>2</sup> ) ± Error			
	SS316L #1	SS316L #2	IN740H #1	IN740H #2
0	16.1913±0.0006	15.6924±0.0005	22.2900±0.0005	22.5735±0.0005

25	16.1914±0.0004	15.6923±0.0006	22.2892±0.0004	22.5723±0.0005
77	16.1920±0.0006	15.6921±0.0006	22.2887±0.0006	22.5722±0.0006
159	16.1917±0.0006	15.6917±0.0003	22.2883±0.0004	22.5716±0.0004
269	16.1916±0.0006	15.6918±0.0006	22.2879±0.0006	22.5707±0.0005
424	16.1912±0.0004	15.6910±0.0002	22.2876±0.0003	22.5709±0.0003
606	16.1914±0.0006	15.6904±0.0007	22.2870±0.0006	22.5702±0.0008
728	16.1905±0.0002	15.7007±0.0001	22.2908±0.0008	22.5706±0.0001
776	16.1915±0.0001	15.6905±0.0003	22.2874±0.0001	22.5702±0.0001
897	16.1912±0.0004	15.6904±0.0003	22.2872±0.0004	22.5700±0.0004
948	16.1905±0.0004	15.6901±0.0003	22.2867±0.0004	22.5692±0.0001

**Table A.5 Specimen mass of test with WED 430 particles and HAY230 specimens at HT. Part 1**

Test Time (hours)	Abrasion Wear (mg/cm <sup>2</sup> ) ± Error					
	HAY230 #1	HAY230 #2	HAY230 #3	HAY230 #4	HAY230 #5	HAY230 #6
0	33.1230±0.0002	33.0837±0.0002	33.0756±0.0002	33.1016±0.0002	33.1772±0.0003	33.1158±0.0002
5	33.1260±0.0003	33.0859±0.0002	33.0771±0.0002	33.0995±0.0002	33.1797±0.0002	33.1175±0.0002
29	33.1263±0.0004	33.0865±0.0003	33.0787±0.0003	33.0996±0.0003	33.1798±0.0003	33.1196±0.0002
41	33.1271±0.0003	33.0877±0.0003	33.0845±0.0003	33.0955±0.0002	33.1805±0.0002	33.1201±0.0001
71	33.1269±0.0001	33.0862±0.0002	33.0788±0.0003	33.0951±0.0002	33.1803±0.0003	33.1199±0.0003
124	33.1269±0.0003	33.0864±0.0002	33.0797±0.0003	33.0956±0.0002	33.1811±0.0004	33.1200±0.0002
196	33.1279±0.0002	33.0872±0.0003	33.0797±0.0003	33.0956±0.0002	33.1810±0.0002	33.1198±0.0002
268	33.1278±0.0001	33.0872±0.0003	33.0797±0.0003	33.0954±0.0002	33.1810±0.0002	33.1199±0.0002
381	33.1287±0.0001	33.0872±0.0002	33.0812±0.0002	33.0959±0.0002	33.1830±0.0002	33.1209±0.0002
480	33.1242±0.0003	33.0836±0.0003	33.0767±0.0003	33.0926±0.0003	33.1791±0.0003	33.1169±0.0003

550	33.1224±0.0004	33.0833±0.0005	33.0748±0.0004	33.0917±0.0004	33.1782±0.0005	33.1149±0.0004
625	33.1216±0.0005	33.0821±0.0004	33.0735±0.0004	33.0908±0.0005	33.1771±0.0005	33.1133±0.0004
727	33.1208±0.0002	33.0818±0.0001	33.0725±0.0002	33.0905±0.0002	33.1769±0.0004	33.1122±0.0002
799	33.1191±0.0002	33.0809±0.0003	33.0715±0.0002	33.0899±0.0002	33.1759±0.0002	33.1111±0.0003
871	33.1187±0.0002	33.0800±0.0002	33.0714±0.0003	33.0892±0.0003	33.1754±0.0003	33.1097±0.0002

Table A.6 is a continuation of Table A.5.

**Table A.6 Specimen mass of test with WED 430 particles and HAY230 specimens at HT. Part 2**

Test Time (hours)	Abrasion Wear (mg/cm <sup>2</sup> ) ± Error	
	HAY230 #7	HAY230 OO
0	33.1178±0.0003	33.9970±0.0003
5	33.1195±0.0002	33.9987±0.0002
29	33.1203±0.0003	33.9995±0.0004
41	33.1207±0.0003	33.9996±0.0002

71	33.1209±0.0002	34.0008±0.0001
124	33.1217±0.0002	34.0010±0.0003
196	33.1211±0.0003	34.0008±0.0002
268	33.1212±0.0003	34.0017±0.0003
381	33.1224±0.0002	34.0021±0.0002
480	33.1189±0.0003	34.0022±0.0004
550	33.1183±0.0004	34.0025±0.0004
625	33.1173±0.0005	34.0024±0.0007
727	33.1170±0.0002	34.0023±0.0002
799	33.1165±0.0002	34.0021±0.0002
871	33.1156±0.0002	34.0019±0.0002

**Table A.7 Specimen mass of test with WED 430 particles and HAY230 specimens at LT. Part 1**

Test Time (hours)	Abrasion Wear (mg/cm <sup>2</sup> ) ± Error					
	HAY230 #1	HAY230 #2	HAY230 #3	HAY230 #4	HAY230 #5	HAY230 #6
0	31.5139±0.0005	31.4801±0.0003	31.4537±0.0008	31.4318±0.0004	31.5151±0.0003	31.6671±0.0004
24	31.5166±0.0013	31.4782±0.0010	31.4516±0.0007	31.4287±0.0007	31.5115±0.0007	31.6640±0.0006
47	31.5124±0.0004	31.4768±0.0004	31.4509±0.0004	31.4283±0.0005	31.5113±0.0004	31.6609±0.0004
94	31.5110±0.0005	31.4761±0.0005	31.4507±0.0003	31.4280±0.0003	31.5097±0.0005	31.6591±0.0004
166	31.5108±0.0003	31.4754±0.0003	31.4503±0.0002	31.4275±0.0004	31.5093±0.0002	31.6581±0.0002
262	31.5087±0.0002	31.4737±0.0002	31.4490±0.0004	31.4270±0.0007	31.5083±0.0002	31.6565±0.0003
406	31.5095±0.0003	31.4743±0.0002	31.4494±0.0003	31.4269±0.0003	31.5082±0.0003	31.6567±0.0004
574	31.5089±0.0003	31.4740±0.0005	31.4486±0.0003	31.4268±0.0003	31.5077±0.0004	31.6561±0.0002
763	31.5088±0.0007	31.4742±0.0009	31.4481±0.0007	31.4264±0.0007	31.5072±0.0007	31.6556±0.0007
910	31.5083±0.0001	31.4734±0.0003	31.4480±0.0000	31.4264±0.0001	31.5063±0.0001	31.6550±0.0001

1027	31.5082±0.0004	31.4736±0.0003	31.4476±0.0004	31.4262±0.0004	31.5069±0.0006	31.6553±0.0003
------	----------------	----------------	----------------	----------------	----------------	----------------

Table A.8 is a continuation of Table A.7.

**Table A.8 Specimen mass of test with WED4 430 particles and HAY230 specimens at LT. Part 2**

Test Time (hours)	Abrasion Wear (mg/cm <sup>2</sup> ) ± Error	
	HAY230 #7	HAY230 #8
0	32.9759±0.0004	33.1083±0.0004
24	32.9743±0.0009	33.1064±0.0008
47	32.9737±0.0004	33.1067±0.0003
94	32.9726±0.0004	33.1057±0.0004
166	32.9724±0.0003	33.1054±0.0003
262	32.9707±0.0004	33.1036±0.0004
406	32.9710±0.0003	33.1042±0.0002

574	32.9706±0.0002	33.1034±0.0002
763	32.9703±0.0007	33.1025±0.0008
910	32.9695±0.0001	33.1024±0.0003
1027	32.9692±0.0007	33.1024±0.0004

**Table A.9 Specimen mass of test with HSP 40/70 #2 particles and SS316L specimens at HT.**

Test Time (hours)	Abrasion Wear (mg/cm <sup>2</sup> ) ± Error			
	SS316L #1	SS316L #2	SS316L #3	SS316L #4
0	16.1238±0.0002	15.8235±0.0005	15.6342±0.0004	15.9346±0.0005
10	16.1242±0.0003	15.8233±0.0005	15.6338±0.0006	15.9352±0.0005
34	16.1245±0.0005	15.8228±0.0008	15.6337±0.0006	15.9349±0.0004
70	16.1236±0.0004	15.8231±0.0007	15.6340±0.0005	15.9346±0.0009
118	16.1233±0.0004	15.8225±0.0007	15.6336±0.0002	15.9343±0.0009
170	16.1234±0.0004	15.8224±0.0003	15.6333±0.0003	15.9345±0.0003

230	16.1228±0.0002	15.8220±0.0004	15.6328±0.0004	15.9338±0.0003
296	16.1226±0.00006	15.8222±0.0002	15.6332±0.0001	15.9336±0.0003
368	16.1225±0.0009	15.8217±0.0003	15.6329±0.0007	15.9332±0.0002
450	16.1222±0.0006	15.8216±0.0003	15.6325±0.0007	15.9329±0.0006
557	16.1216±0.0006	15.8214±0.0007	15.6321±0.0006	15.9329±0.0004
628	16.1217±0.000	15.8208±0.0007	15.6323±0.0006	15.9328±0.0005
702	16.1209±0.000	15.8209±0.0008	165.6322±0.0006	15.9327±0.0003

**Table A.10 Specimen mass of test with WED 430 particles and SS316L and SS316H specimens at HT. Part 1**

Test Time (hours)	Abrasion Wear (mg/cm <sup>2</sup> ) ± Error					
	SS316L #1	SS316L #2	SS316L #3	SS316L #4	SS316H #1	SS316H #2
0	15.6329±0.0002	15.7510±0.0003	16.1595±0.0002	15.8000±0.0002	22.6016±0.0002	22.9276±0.0002
5	15.6350±0.0002	15.7523±0.0003	16.1635±0.0002	15.8012±0.0003	22.5867±0.0003	22.9145±0.0003

29	15.6366±0.0003	15.7543±0.0003	16.1626±0.0003	15.8026±0.0002	22.5711±0.0003	22.8977±0.0002
57	15.6369±0.0002	15.7544±0.0003	16.1628±0.0002	15.8031±0.0003	22.5690±0.0002	22.8939±0.0002
112	15.6361±0.0002	15.7541±0.0003	16.1619±0.0002	15.8038±0.0002	22.5681±0.0002	22.8929±0.0002
184	15.6339±0.0001	15.7545±0.0002	16.1609±0.0004	15.8038±0.0002	22.5672±0.0002	22.8924±0.0002
287	15.6313±0.0004	15.7537±0.0002	16.1585±0.0002	15.8050±0.0004	22.5665±0.0002	22.8914±0.0002
391	15.6304±0.0003	15.7535±0.0003	16.1583±0.0003	15.8058±0.0003	22.5668±0.0003	22.8911±0.0003
520	15.6289±0.0002	15.7530±0.0003	16.1567±0.0002	15.8054±0.0002	22.5651±0.0002	22.8902±0.0002
630	15.6298±0.0002	15.7524±0.0002	16.1582±0.0001	15.8058±0.0001	22.5646±0.0001	22.8897±0.0001
737	15.6296±0.0003	15.7541±0.0003	16.1568±0.0003	15.8072±0.0003	22.5648±0.0003	22.8912±0.0003

Table A.11 is a continuation of Table A.10.

Table A.11 Specimen mass of test with WED 430 particles and SS316L and SS316H specimens at HT. Part 2

Test Time (hours)	Abrasion Wear (mg/cm <sup>2</sup> ) ± Error					
	SS316H #3	SS316H #4	SS316L OO	SS316H OO	SS316L OO	SS316H OO
0	22.5782±0.0003	22.8802±0.0003	16.3595±0.0003	22.8746±0.0002	16.3617±0.0002	22.8731±0.0003
5	22.5691±0.0002	22.8658±0.0003	16.3636±0.0002	22.8107±0.0003	16.3638±0.0002	22.8092±0.0002
29	22.5405±0.0002	22.8516±0.0002	16.3641±0.0001	22.8099±0.0002	16.3640±0.0002	22.8095±0.0002
57	22.5383±0.0002	22.8447±0.0002	16.3644±0.0002	22.8091±0.0003	16.3657±0.0003	22.8095±0.0003
112	22.5377±0.0001	22.8442±0.0002	16.3642±0.0002	22.8079±0.0002	16.3650±0.0002	22.8082±0.0002
184	22.5371±0.0003	22.8434±0.0003	16.3653±0.0003	22.8081±0.0003	16.3653±0.0003	22.8081±0.0003
287	22.5363±0.0002	22.8423±0.0002				
391	22.5362±0.0004	22.8423±0.0004				
520	22.5346±0.0002	22.8407±0.0002				
630	22.5321±0.0001	22.8418±0.0001				
737	22.5306±0.0003	22.8421±0.0003				

Table A.12 Specimen mass of test with WED 430 particles and SS316L and SS316H specimens at LT. Part 1

Test Time (hours)	Abrasion Wear (mg/cm <sup>2</sup> ) ± Error									
	SS316L #1	SS316L #2	SS316L #3	SS316L #4	SS316H #1	SS316H #2				
0	15.6457±0.0003	16.1690±0.0002	15.1491±0.0003	15.4848±0.0005	22.8681±0.0003	22.6303±0.0002				
35	15.6446±0.0007	16.1670±0.0004	15.1481±0.0004	15.4844±0.0006	22.8671±0.0004	22.6292±0.0004				
107	15.6441±0.0001	16.1670±0.0001	15.1474±0.0002	15.4836±0.0002	22.8665±0.0002	22.6284±0.0003				
161	15.6437±0.0001	16.1657±0.0001	15.1466±0.0001	15.4837±0.0001	22.8663±0.0002	22.6279±0.0002				
233	15.6436±0.0002	16.1657±0.0003	15.1461±0.0002	15.4834±0.0004	22.8660±0.0003	22.6279±0.0003				
288	15.6429±0.0004	16.1649±0.0004	15.1457±0.0001	15.4833±0.0002	22.8656±0.0002	22.6277±0.0002				
343	15.6427±0.0003	16.1654±0.0002	15.1459±0.0002	15.4830±0.0002	22.8655±0.0001	22.6273±0.0002				
373	15.6425±0.0003	16.1647±0.0002	15.1458±0.0002	15.4828±0.0002	22.8655±0.0002	22.6269±0.0004				
405	15.6422±0.0002	16.1646±0.0002	15.1456±0.0002	15.4829±0.0002	22.8653±0.0002	22.6272±0.0003				
523	15.6421±0.0002	16.1646±0.0003	15.1453±0.0003	15.4828±0.0003	22.8655±0.0003	22.6273±0.0002				

651	15.6427±0.0002	16.1646±0.0002	15.1454±0.0003	15.4828±0.0002	22.8655±0.0002	22.6273±0.0003
791	15.6425±0.0003	16.1642±0.0002	15.1453±0.0002	15.4825±0.0002	22.8652±0.0001	22.6275±0.0001

Table A.13 is a continuation of Table A.12.

**Table A.13 Specimen mass of test with WED 430 particles and SS316L and SS316H specimens at LT. Part 2**

Test Time (hours)	Abrasion Wear (mg/cm <sup>2</sup> ) ± Error	
	SS316H #3	SS316H #4
0	22.8316±0.0002	22.9189±0.0004
35	22.8309±0.0006	22.9178±0.0004
107	22.8309±0.0001	22.9177±0.0004
161	22.8302±0.0001	22.9171±0.0001
233	22.8301±0.0002	22.9167±0.0002
288	22.8297±0.0003	22.9164±0.0003

343	22.8299±0.0002	22.9162±0.0002
373	22.8296±0.0002	22.9159±0.0002
405	22.8296±0.0002	22.9161±0.0002
523	22.8298±0.0003	22.9161±0.0003
651	22.8299±0.0002	22.9160±0.0002
791	22.8298±0.0001	22.9159±0.0001

APPENDIX B

Appendix B shows figures of surface profilometry for SS316L. Images are taken in the middle of the surface.

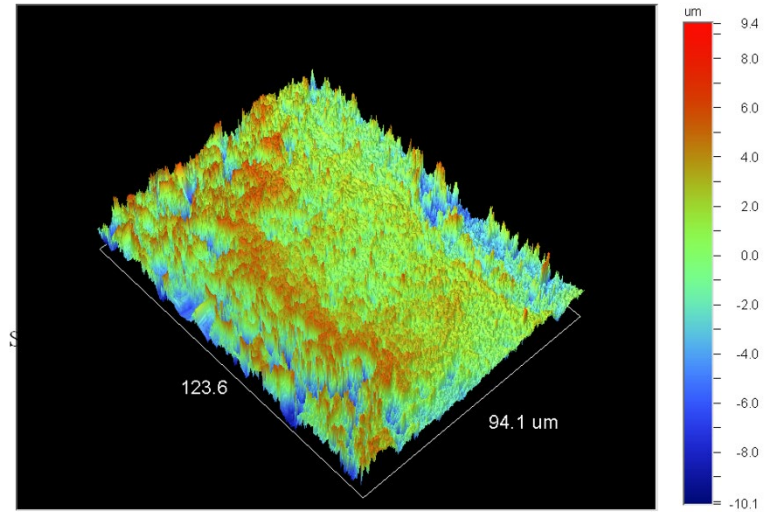


**Figure B.1** Surface profilometry of SS316L middle surface untested.

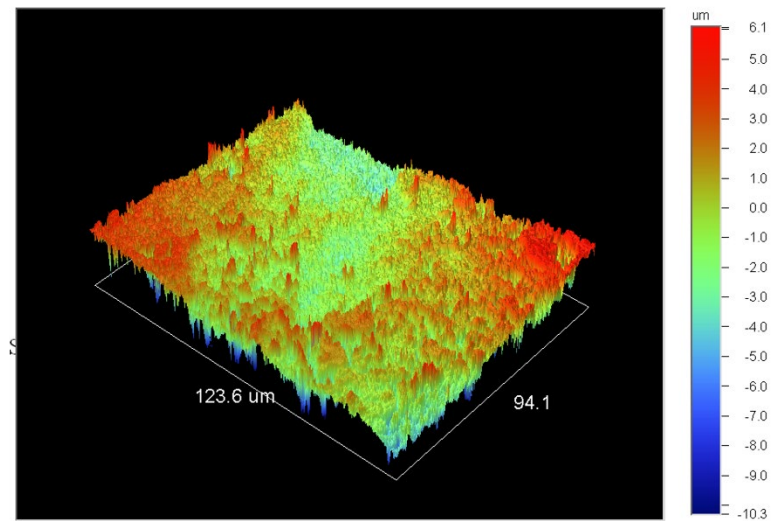


**Figure B.2** Surface profilometry of SS316L middle surface through HSP 40/70 particles.

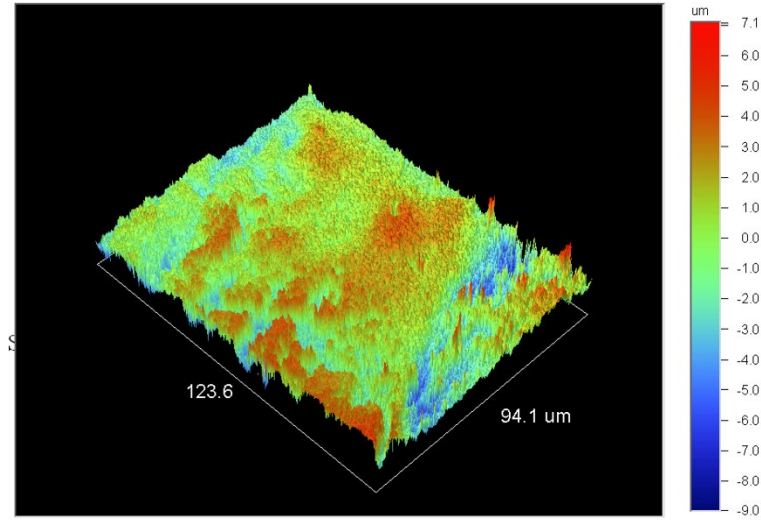


**Figure B.3** Surface profilometry of SS316L middle surface through MAX HD 35 particles.

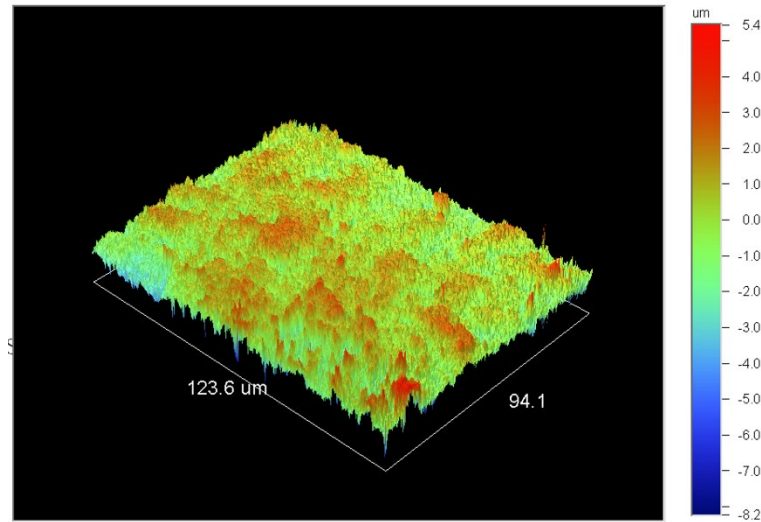


**Figure B.4** Surface profilometry of SS316L middle surface through WED 430 particles.